Karlsruhe Institute of Technology

WindForS
Wind Energy
Research Alliance

Mixing-layer height and low-level jets

Stefan Emeis
stefan.emeis@kit.edu

INSTITUTE OF METEOROLOGY AND CLIMATE RESEARCH, Atmospheric Environmental Research

Introduction

- definition of mixing layer

- definition of low-level jet

- relevance for wind energy

- remote sensing

 stefan.emeis@kit.edu Institute for Meteorology and Climate Research – Atmospheric Environmental Research

Mixing-layer height

Inversion height	literally: inversion in the temperature profile, increase of temperature with height, strong decrease of moisture, radiation inversions, sinking inversions, surface inversions, lifted inversions
Mixing-layer height (mixing height, mixed-layer height)	upper boundary for vertical exchange (mixing), upper boundary of the well-mixed layer, entrainment, defined by the turbulence profile or by the vertical distribution of a tracer (aerosol, pot. temperature)
Boundary layer height	SBL: at night, height of the near-surface layer influenced by surface friction CBL: at day, height of convective plumes

boundary layer height $\approx$ mixing-layer height

boundary layer height $\geq$ inversion height

Mixing-layer height influences diurnal variation of vertical wind profiles

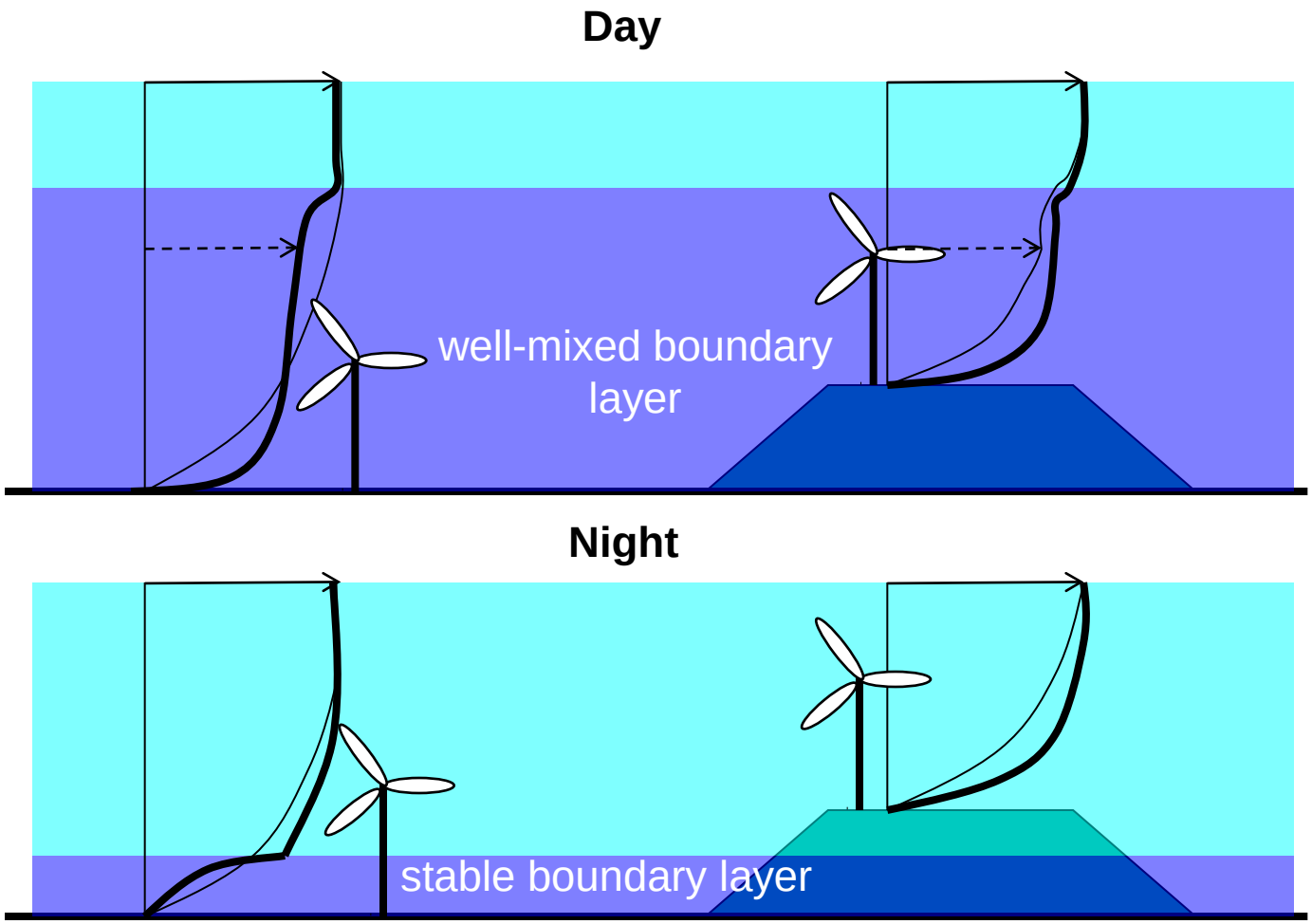

Low-level jet

vertical profiles of wind speed

26 June 2005

AdP Ch d G

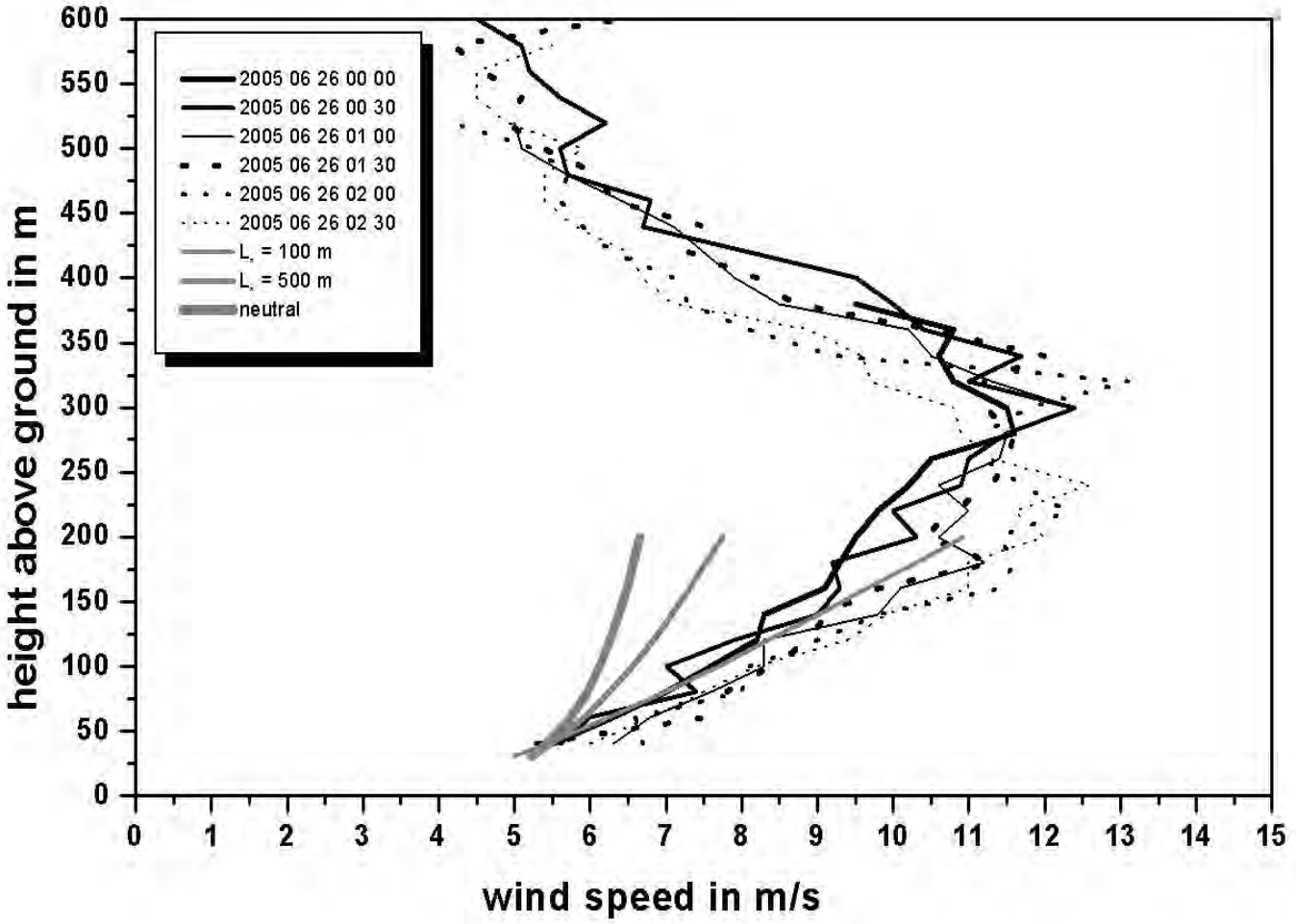

Nocturnal low-level jet and the turning of wind direction with height

Day

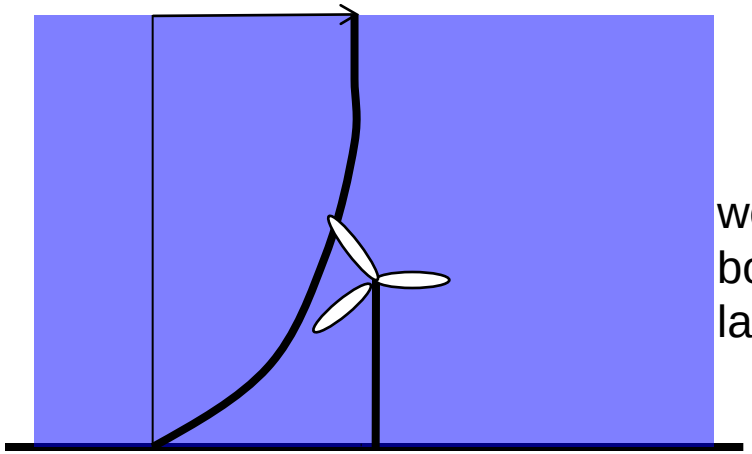

well-mixed boundary layer

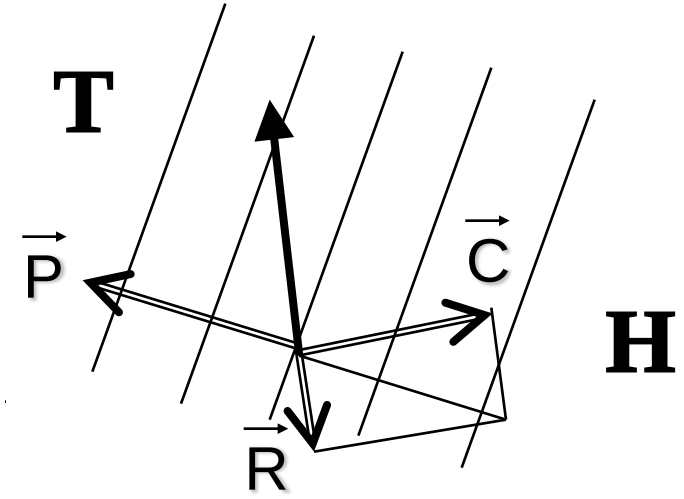

Night

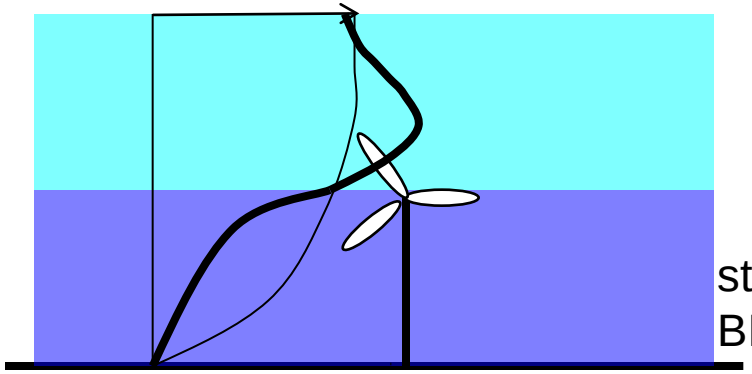

stable BL

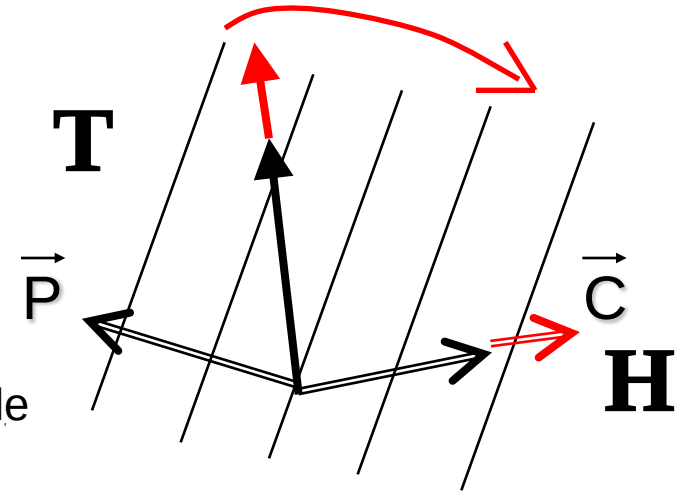

surface pressure
00 GMT

26 June 2005

asterisk denotes location where LLJ was observed

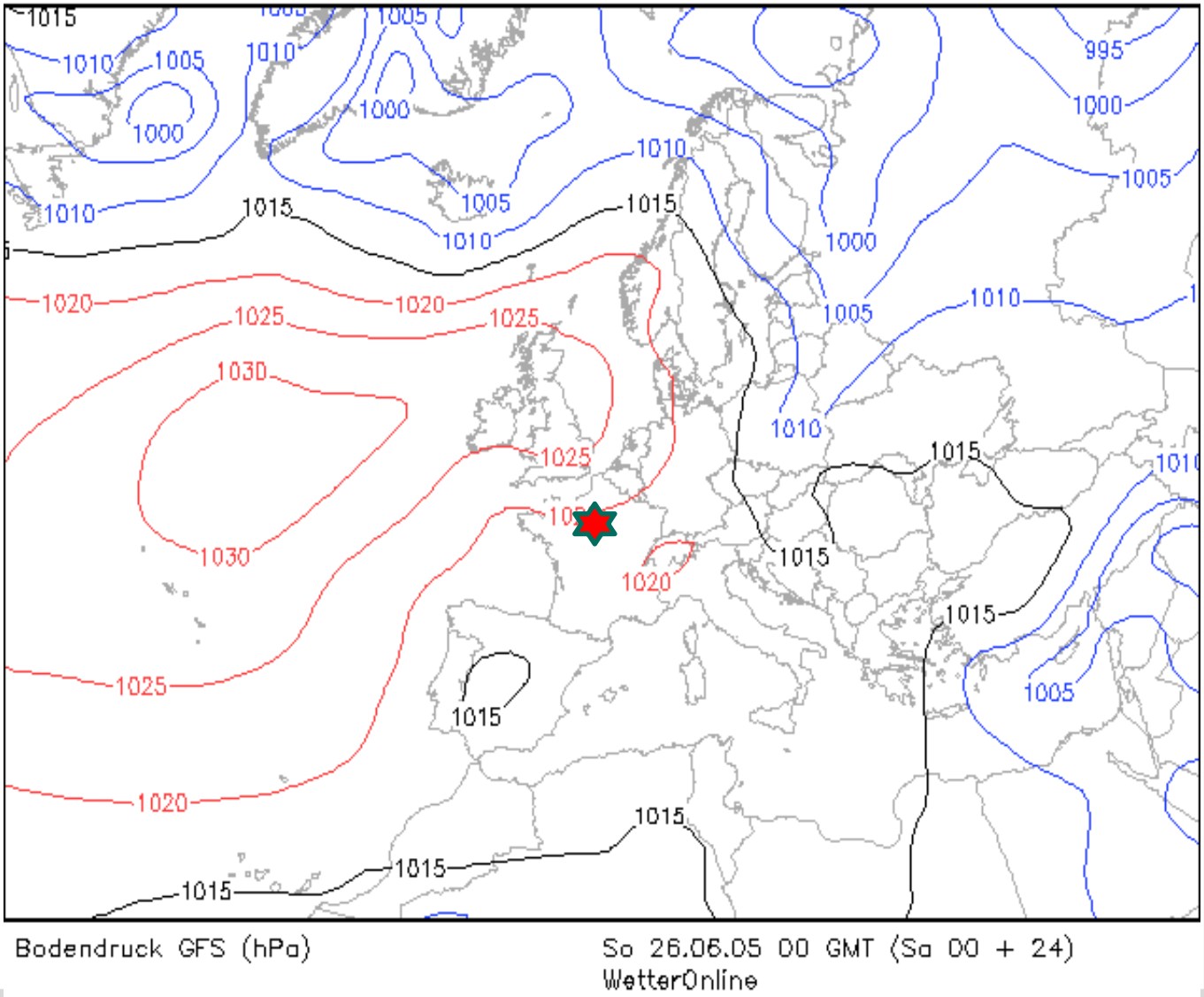

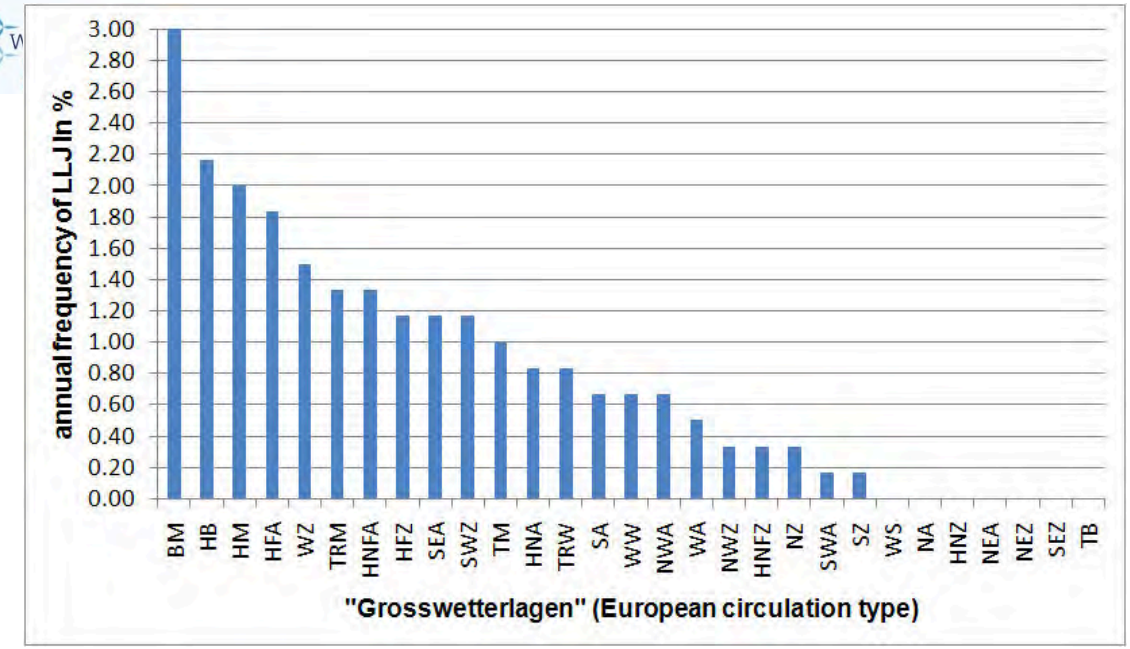

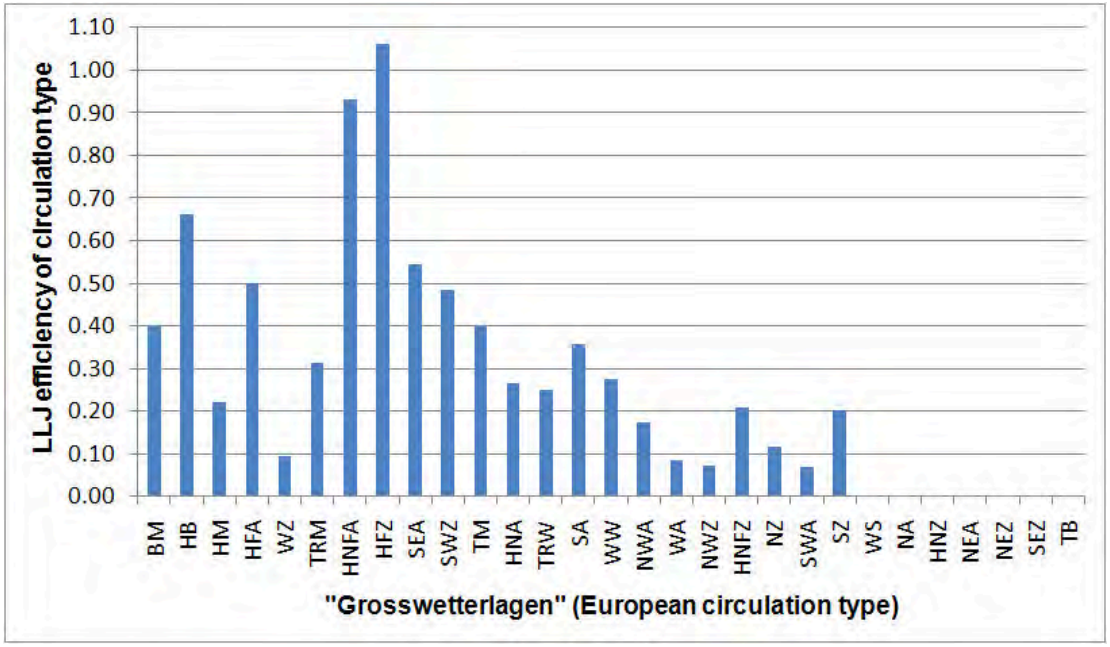

frequency of LLJ over Hanover for 20 months in the years 2001 to 2003

total is 23.17% of all nights

circulation types:

BM ridge over Central Europe
HB high over British Isles
HM high over Central Europe
...

HFZ high over Scandinavia
HNFA high over North Atlantic
...

“efficiency” of a circulation type to produce a LLJ over Hanover for 20 months in the years 2001 to 2003

Relevance for wind energy

The vertical wind profile (equilibrium conditions)

logarithmic law
(with stability correction) $u(z) = (u_*/\kappa)\,(\ln(z/z_0) - \psi(z/L_*))$

power law $u(z) = u(z_A)\,(z/z_A)^n$

New proposal
(Gryning et al. 2007)

$$u(z) = \frac{u_{*0}}{\kappa}\left(\ln\left(\frac{z}{z_0}\right) + \frac{z}{L_{MBL,N}} - \frac{z}{z_i}\left(\frac{z}{2L_{MBL,N}}\right)\right)$$

needs information on the PBL or mixing-layer height

Gryning, S.-E., E. Batchvarova, B. Brümmer, H. Jørgensen, S. Larsen, 2007: On the extension of the wind profile over homogeneous terrain beyond the surface boundary layer. Bound.-Lay. Meteorol., **124**, 251–268.

Peña, A., S.-E. Gryning, C.B. Hasager, 2010: Comparing mixing-length models of the diabatic wind profile over homogeneous terrain. Theor. Appl. Climatol., **100**, 325-353.

LLJ can only be described by time-dependent equations!

Basic remote sensing techniques

subject of this lecture

name	princple	spatial resolution	direction	type
RADAR	backscatter, electro-magnetic pulses, fixed wave length	profiling	scanning, slanted	active, monostatic
SODAR	backscatter, acoustic pulses, fixed wave length	profiling	fixed, slanted, vertical	active, usually monostatic
LIDAR ceilometer	backscatter, optical pulses, fixed wave length(s)	profiling	scanning, fixed, horizontal, slanted, vertical	active, monostatic
RASS	backscatter, acoustic, electro-magnetic, fixed wave length	profiling	fixed, vertical	active, monostatic
FTIR	absorption, infrared, spectrum	path-averaging	fixed, horizontal, slanted	active, bistatic or passive
	emission, infrared, spectrum	path-averaging	fixed, horizontal, slanted	passive
DOAS	absorption, optical, fixed wave lengths	path-averaging	fixed, horizontal	active, bistatic
radiometry	electro-magnetic, fixed wave length(s)	averaging, profiling	fixed, scanning, slanted, vertical	passive
tomography	travel time, acoustic, fixed wave length	horizontal distribution	fixed, horizontal	active, multiple emitters and receivers

subject of this lecture

Frequencies for atmospheric remote sensing

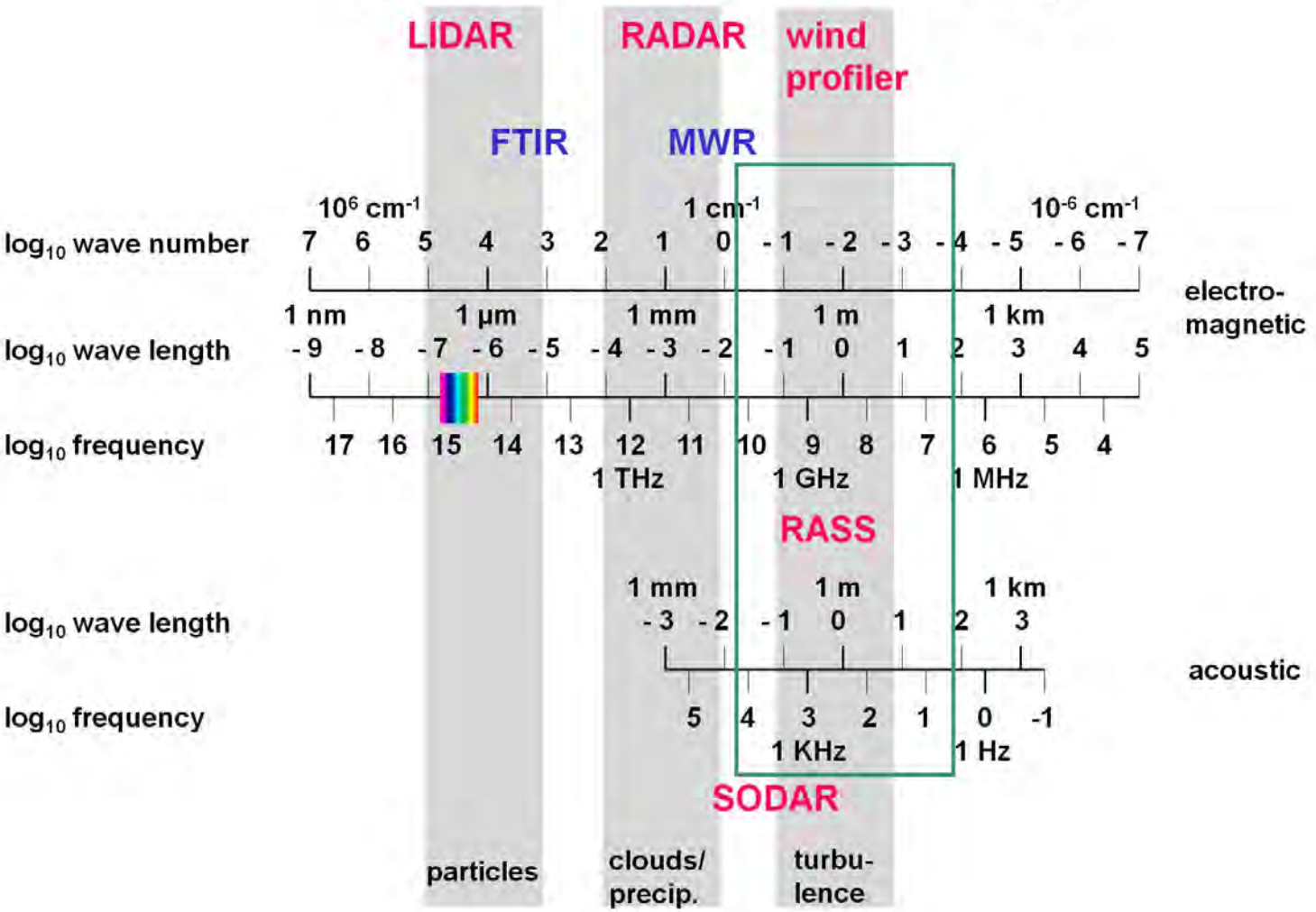

Emeis, S., 2010: Measurement Methods in Atmospheric Sciences - In situ and remote. Borntraeger, Stuttgart, 272 pp., 103 figs, 28 tables, ISBN 978-3-443-01066-9.

Surface-based Remote Sensing Systems

at IMK-IFU

SODAR (Large system), acoustic backscatter, Doppler shift analysis ➔ wind, turbulence

SODAR-RASS (Doppler-RASS), acoustic, electro-magnetic backscatter, determines speed of sound ➔ wind and temperature profiles

Ceilometer, backscatter, optical pulses, wave length ~ 0.9 µm ➔ aerosol profiles

Wind-LIDAR, optical backscatter, Doppler shift analysis, wave length ~ 1.5 µm ➔ wind and aerosol profiles

image: Halo Photonics

SODAR

algorithms for the determination of mixing-layer height

and low-level jet observations

stefan.emeis@kit.edu Institute for Meteorology and Climate Research – Atmospheric Environmental Research

monostatic SODAR: measuring principles

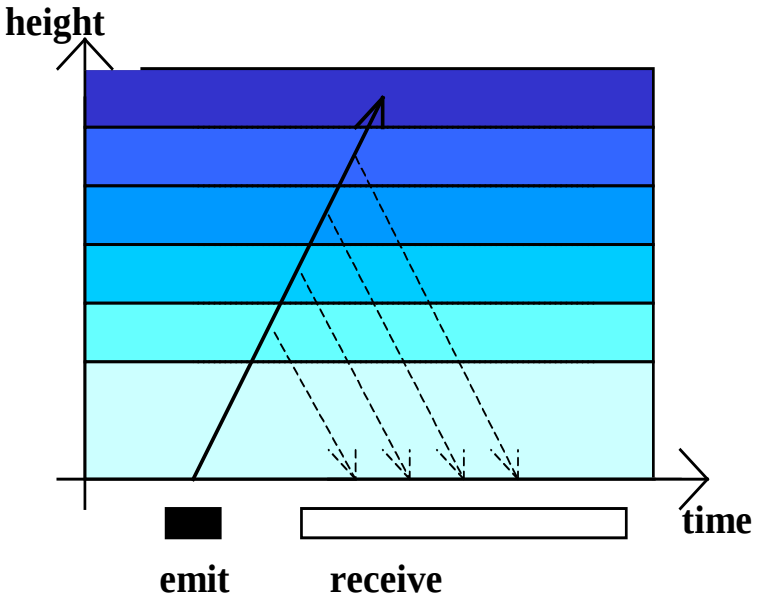

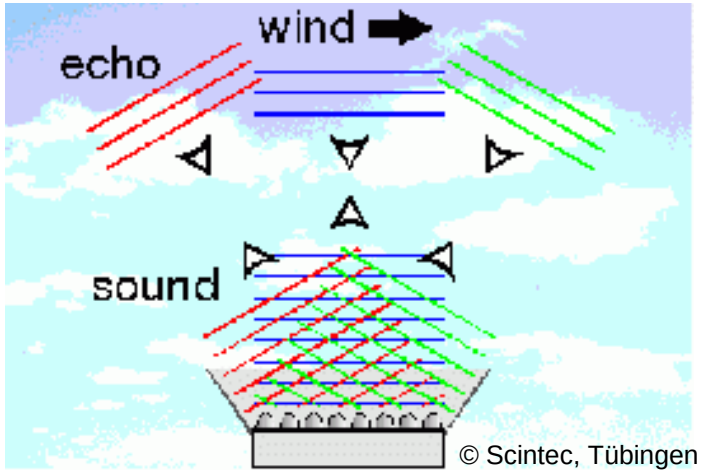

deduction:

sound travel time	=	height
backscatter intensity	=	turbulence
Doppler-shift	=	wind speed

Emission of sound waves into three directions:

in order to measure all three components of the wind (horizontal and vertical)

The SODAR equation:

$$P_R = r^{-2} (c_s \tau A \varepsilon/2) P_0 \beta_s e^{-2\sigma r} + P_{bg}$$

P_R received power,
P_0 emitted power,
ε antenna efficiency,
A effective antenna area,
σ sound absorption in air due to classical and molecular absorption due to the collision of water molecules with the oxygen and nitrogen molecules of the air,
r distance between the scattering volume and the instrument,
τ pulse duration (typically between 20 and 100 ms),
β_s backscattering cross-section (typically in the order of 10^{-11} m^{-1} sr^{-1}),
c_s sound speed,
P_{bg} background noise.

Emitted power: ~ 10^3 W, received (backscattered) power: 10^{-15} W

The SODAR equation:

$$P_R = r^{-2} (c_s \tau A \varepsilon/2) P_0 \beta_s e^{-2\sigma r} + P_{bg}$$

The ratio of the two terms on the right-hand side of the SODAR equation is called signal-to-noise ratio (usually abbreviated as SNR).

The backscattering cross-section β_s is a function of the temperature structure function C_T^2 (Tatarskii 1961).

For a monostatic SODAR we find (Reitebuch 1999) when using the wave number $k = 2\pi/\lambda$:

$$\beta_s(180°) = 0{,}00408\, k^{1/3}\, C_T^2 / T^2$$

Reitebuch, O., 1999: SODAR-Signalverarbeitung von Einzelpulsen zur Bestimmung hochaufgelöster Windprofile. Schriftenreihe des Fraunhofer-Instituts für Atmosphärische Umweltforschung, Shaker Verlag GmbH Aachen, Bd. 62, 178 S.

Tatarskii, V.I., 1971: The effect of the turbulent atmosphere on wave propagation. Kefer Press, Jerusalem, 472 S.

SODAR sample plot (daytime convective BL)

acoustic backscatter intensity

sigma w

40 – 300 m

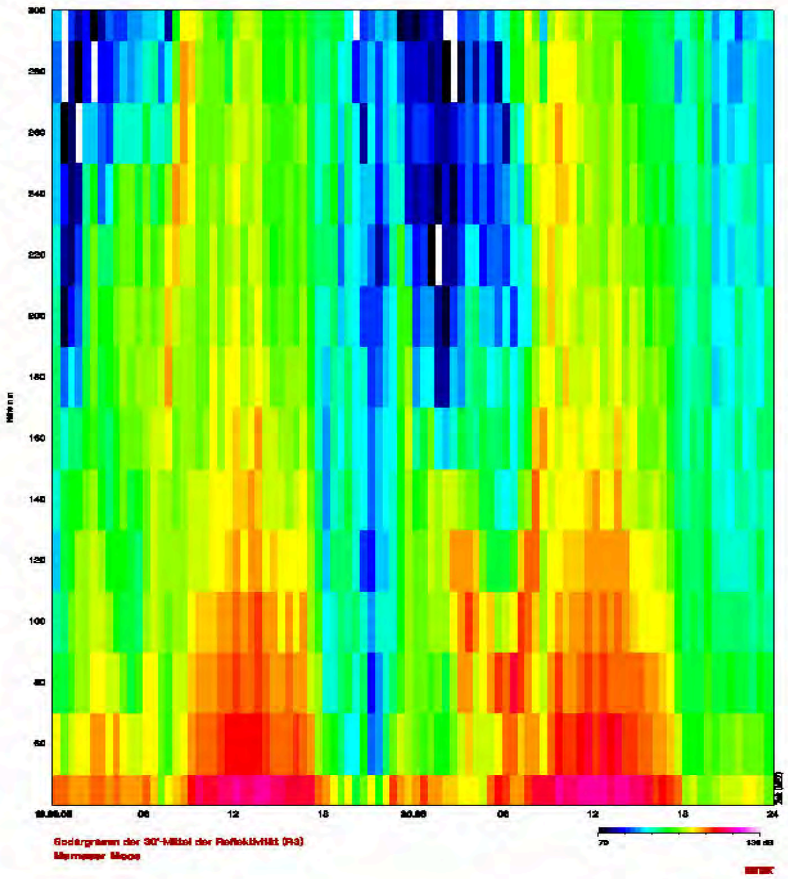

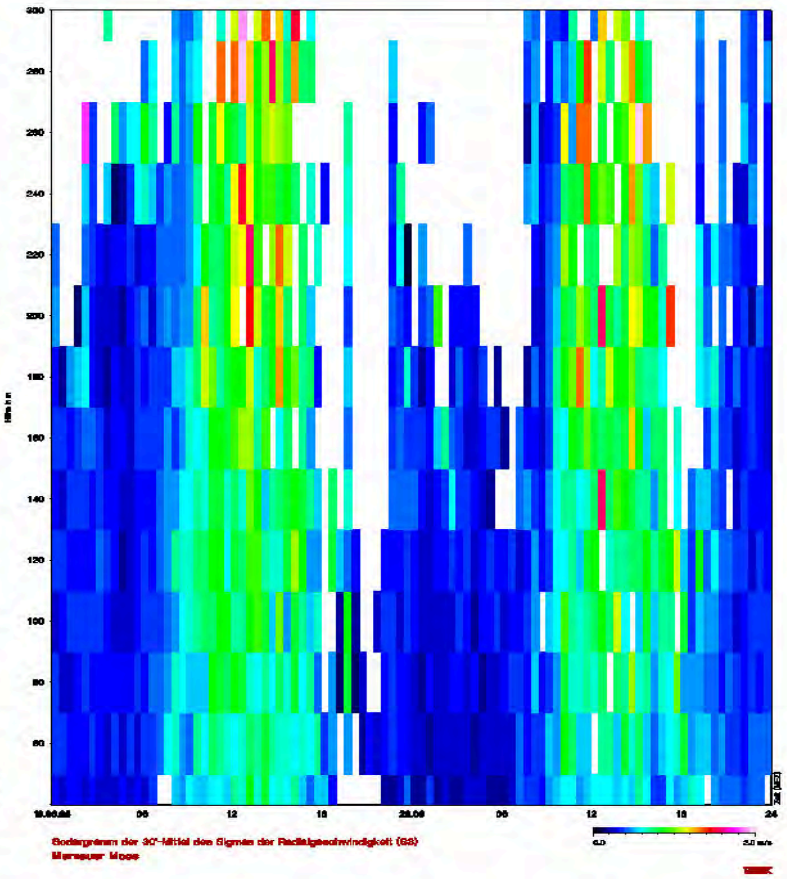

2 days, midnight to midnight

SODAR sample plot (lifted inversion)

acoustic backscatter intensity

sigma w

40 – 400 m

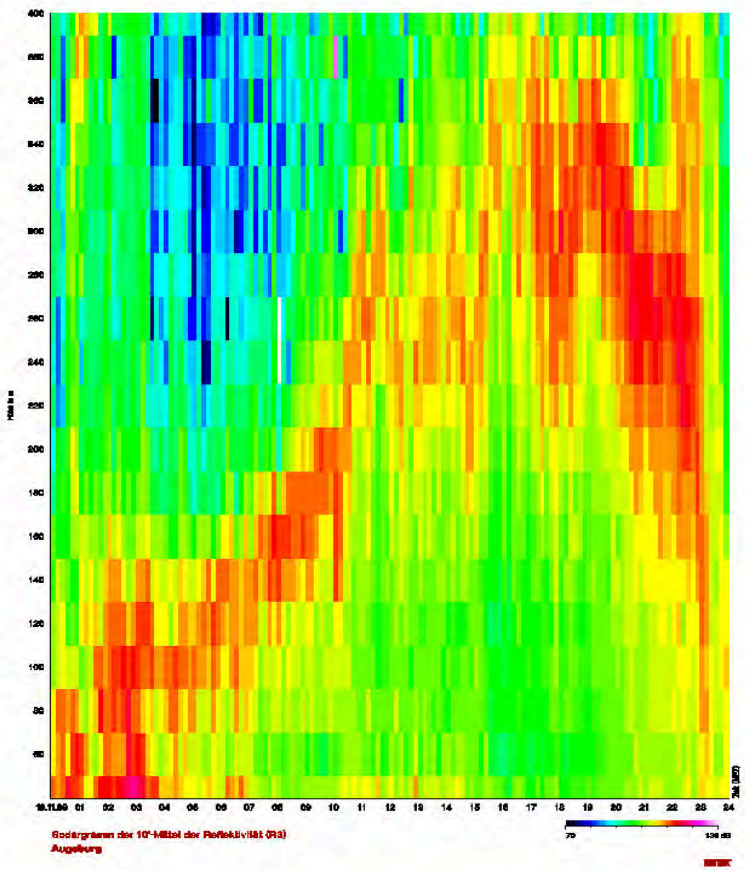

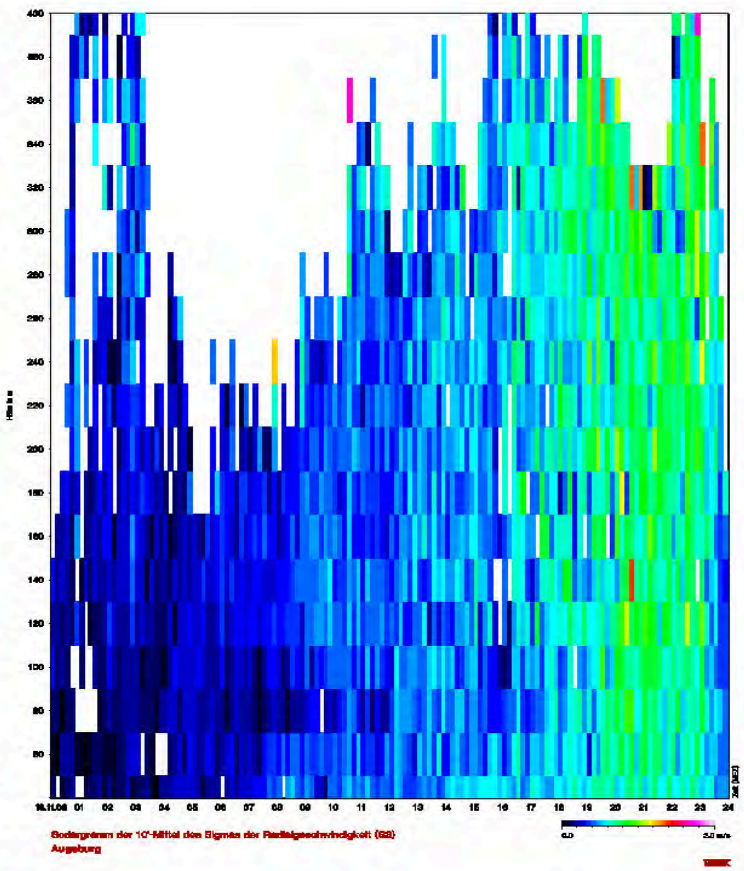

1 day, midnight to midnight

Algorithms to detect MLH from SODAR data

criterion 1:
upper edge of high turbulence

criterion 2:
surface and lifted inversions

MLH = Min (C1, C2)

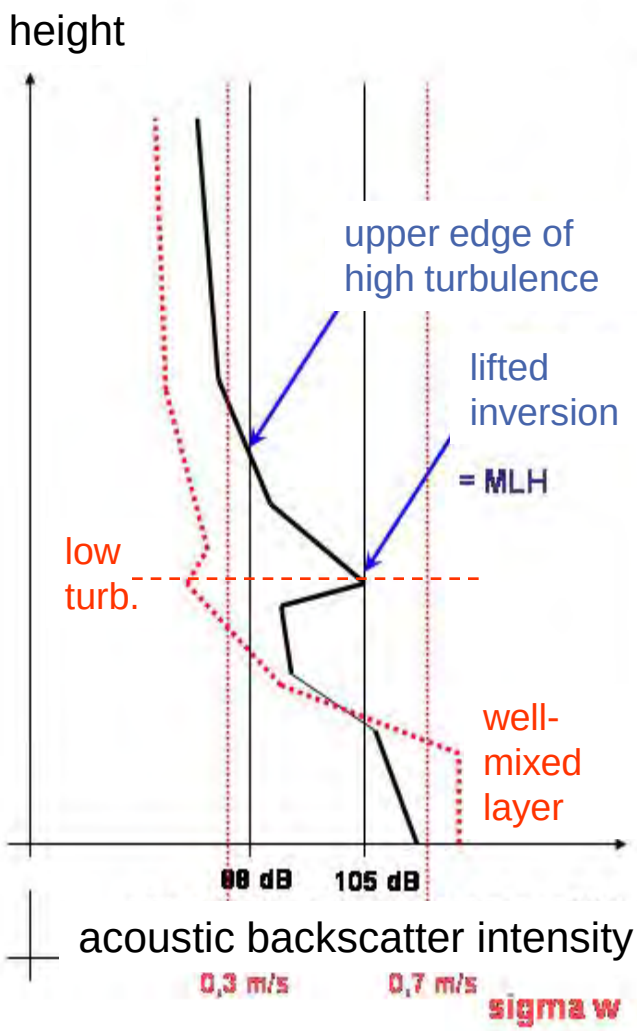

example 1: daytime

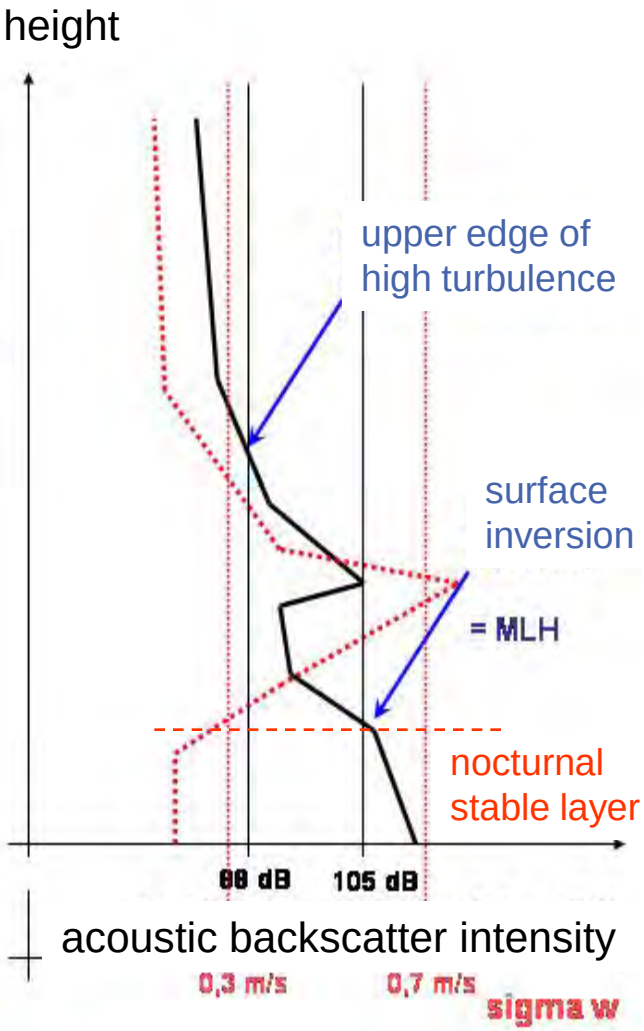

example 2: night-time

Emeis, S., K. Schäfer, C. Münkel, 2008: Surface-based remote sensing of the mixing-layer height – a review. Meteorol. Z., **17**, 621-630.

examples for low-level jet observations with SODAR

vertical profiles of wind speed (30 min means)

23-30 June 2005

AdP Ch d G

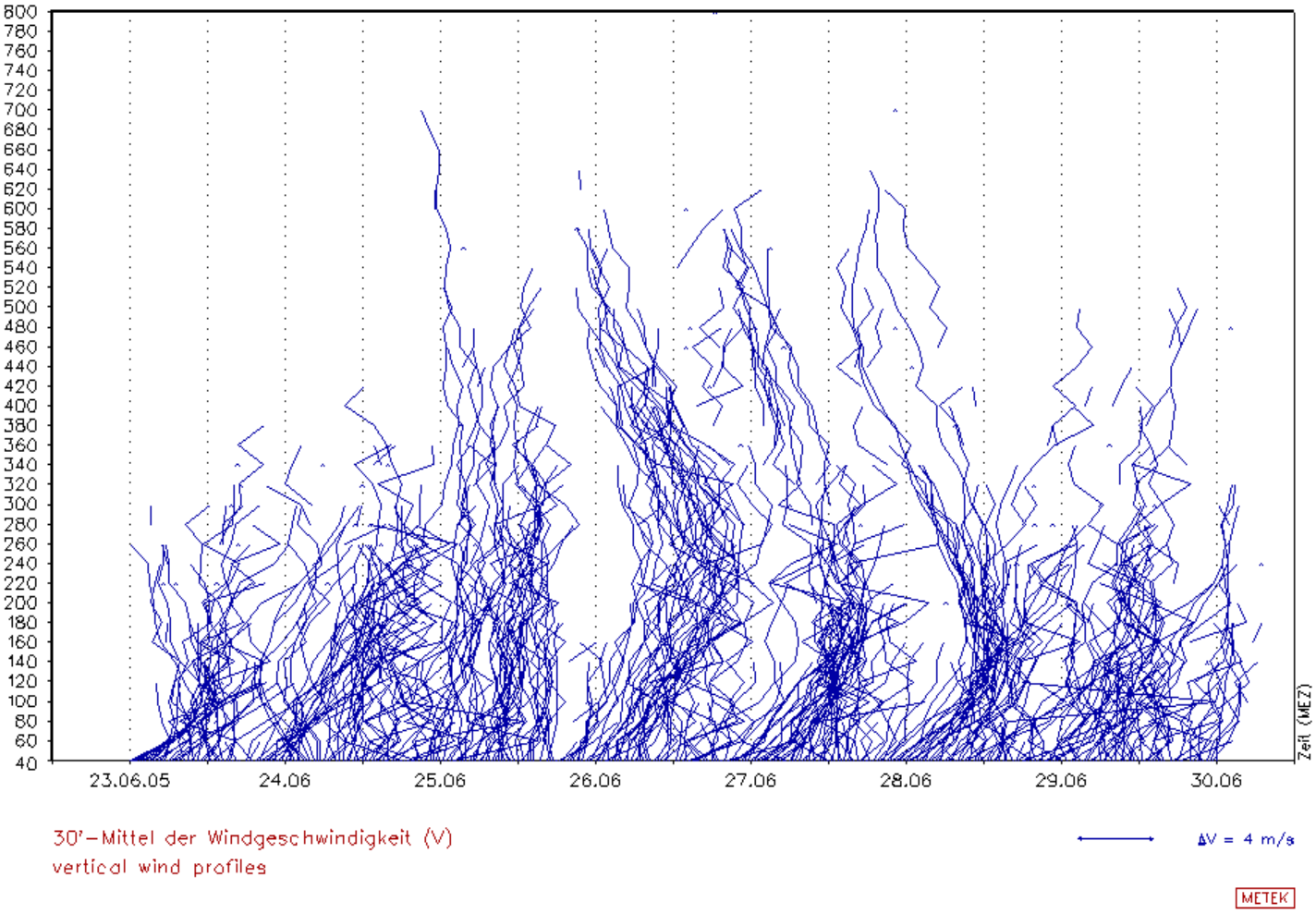

examples for low-level jet observations with SODAR

vertical profiles of wind direction

26 June 2005

AdP Ch d G

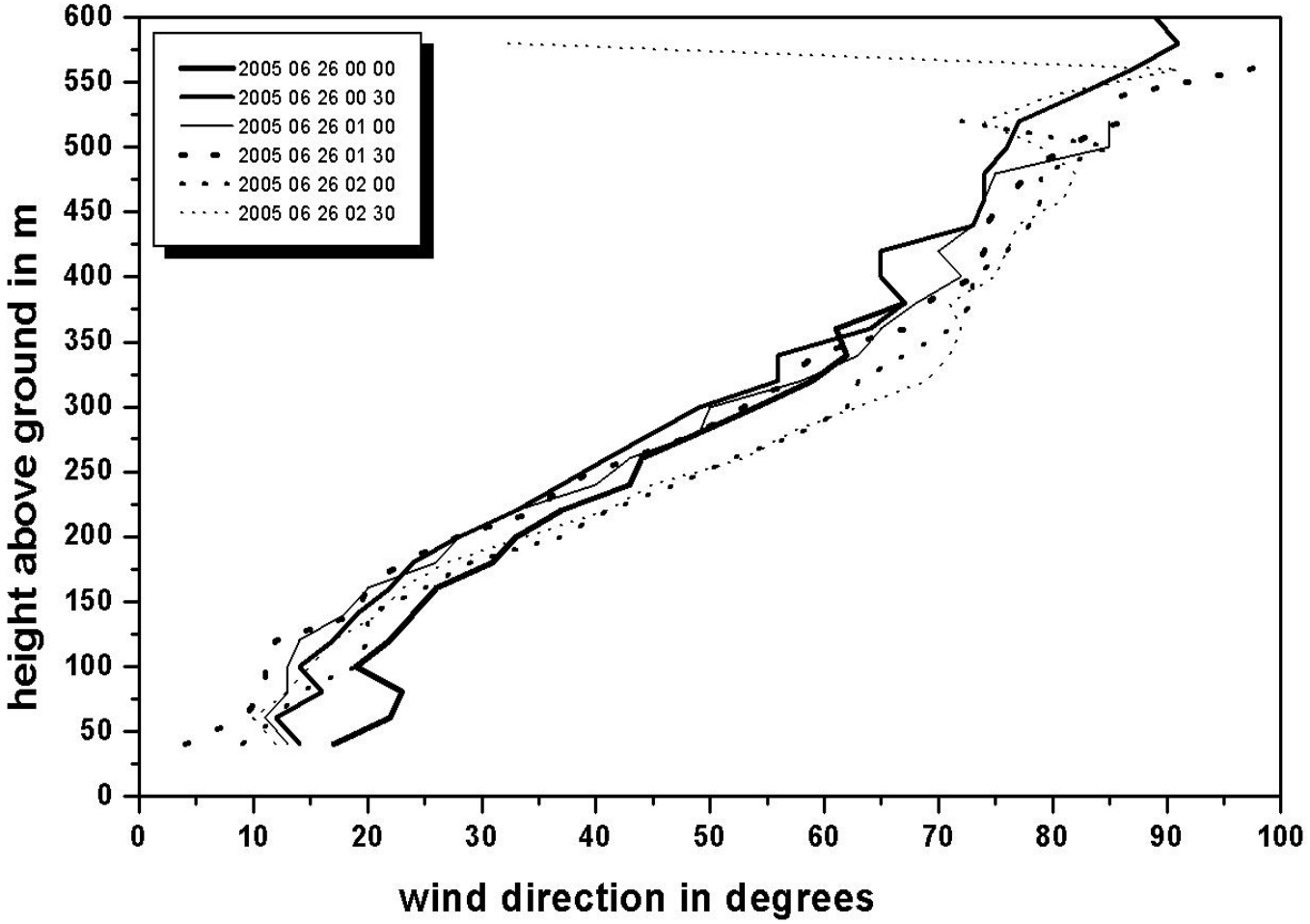

Monthly mean diurnal course of wind speed

August 2002, 17 nights with LLJ

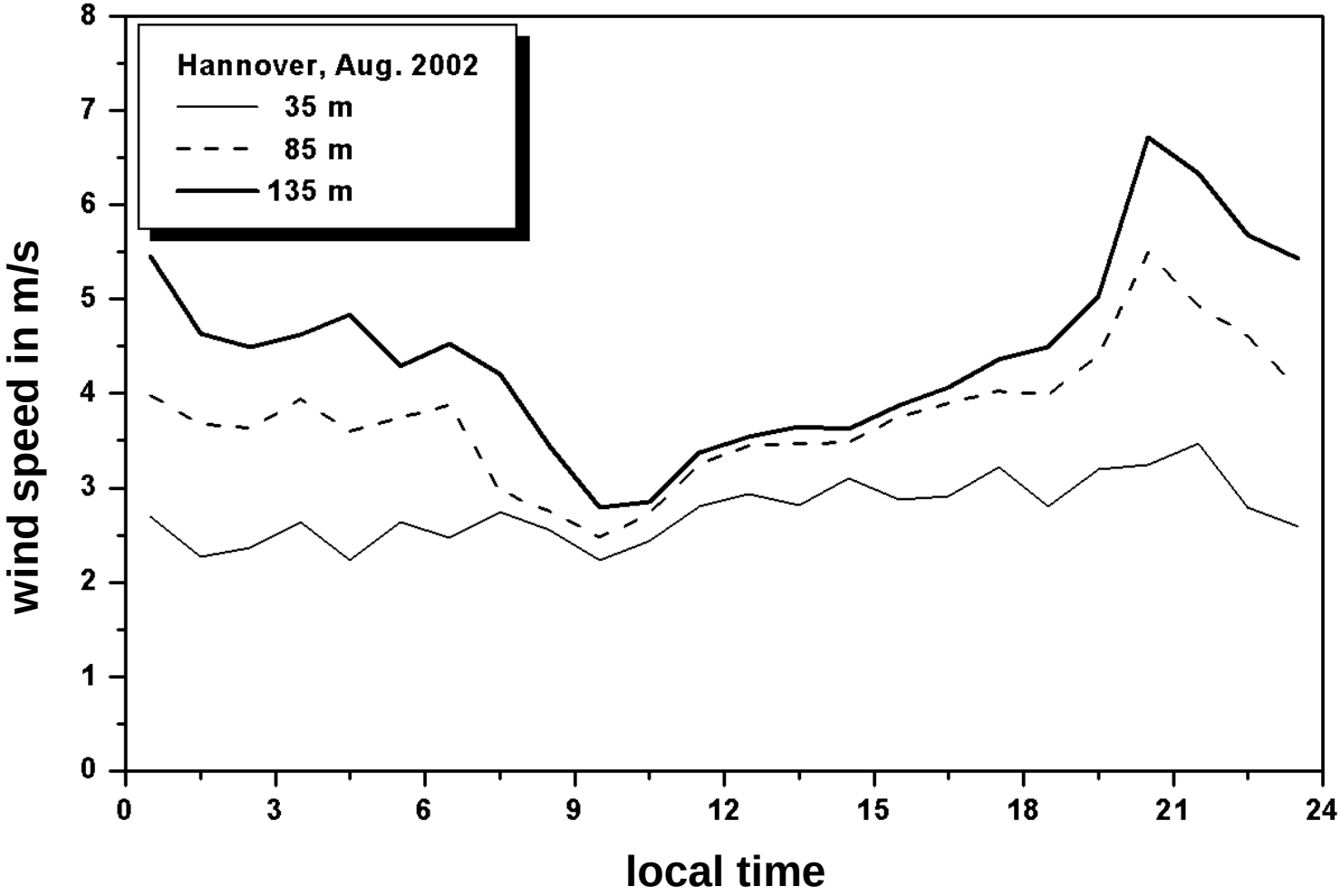

Mean diurnal variation of the turning of wind direction with height

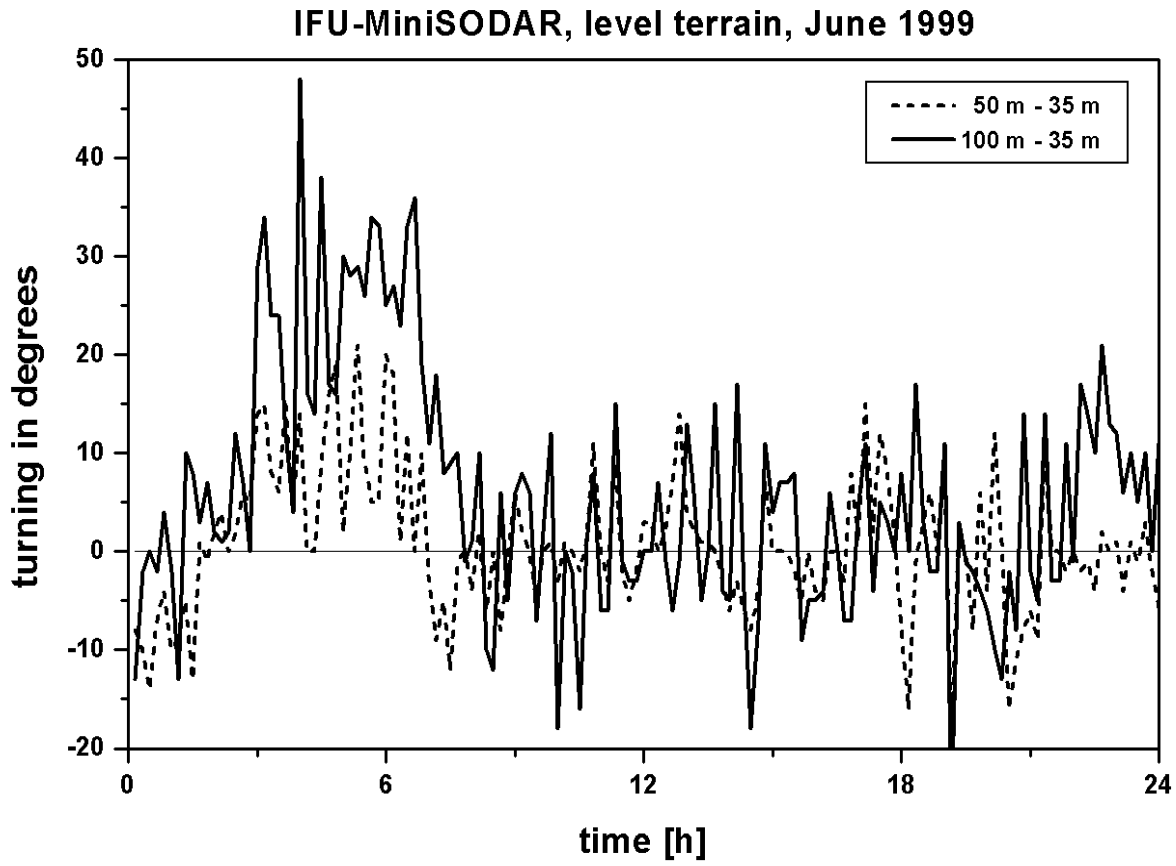

Emeis, S., 2001: Vertical variation of frequency distributions of wind speed in and above the surface layer observed by sodar. Meteorol. Z., **10**, 141-149.

Ceilometer

algorithms for the determination of mixing-layer height

stefan.emeis@kit.edu Institute for Meteorology and Climate Research – Atmospheric Environmental Research

Ceilometer/LIDAR measuring principle

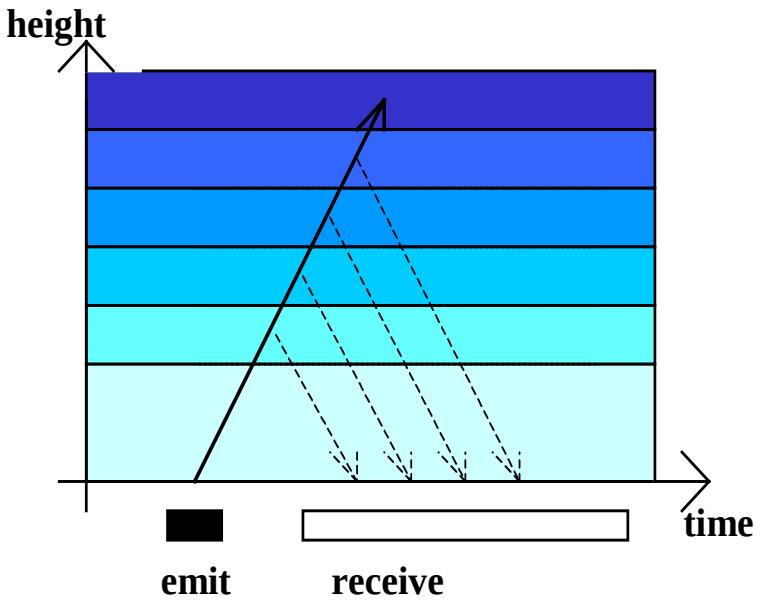

detection:

travel time of signal = height
backscatter intensity = particle size and number distribution
Doppler-shift = cannot be analyzed from ceilometer data
(available only from a Wind-LIDAR: velocity component in line of sight)

The LIDAR equation:

$$P_R(\lambda,r) = r^{-2}\,(c\tau A\varepsilon/2)\,P_0\,[\beta_m(\lambda,r) + \beta_p(\lambda,r)]\,e^{-2\sigma r} + P_{bg}$$

- r distance between the LIDAR and the backscattering object,
- c speed of light,
- τ pulse duration,
- A antenna area,
- ε correction term for the detector efficiency and losses due to the lenses,
- P_0 emitted energy,
- β_m backscatter coefficient for molecules
- β_p backscatter coefficient for particles,
- σ absorption of light in the atmosphere,
- P_{bg} background noise.

For a ceilometer β_m is negligible and only β_p is important

ceilometer sample plot (daytime convective BL)

optical backscatter intensity

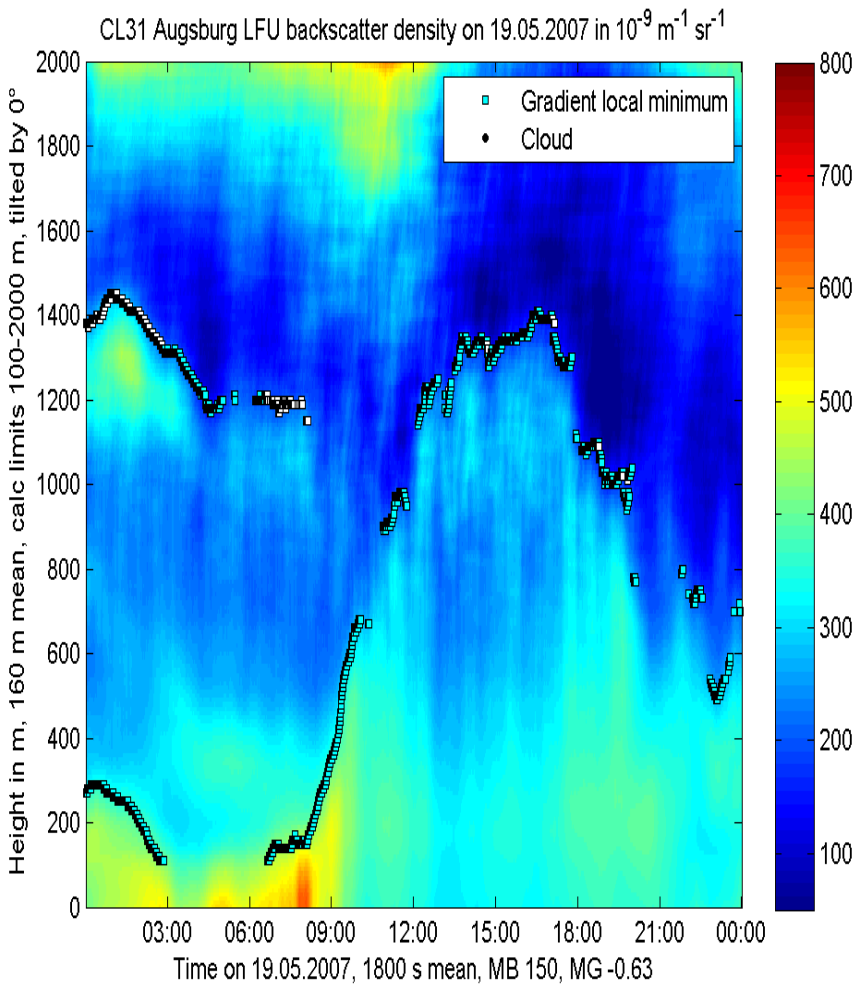

negative vertical gradient of optical backscatter intensity

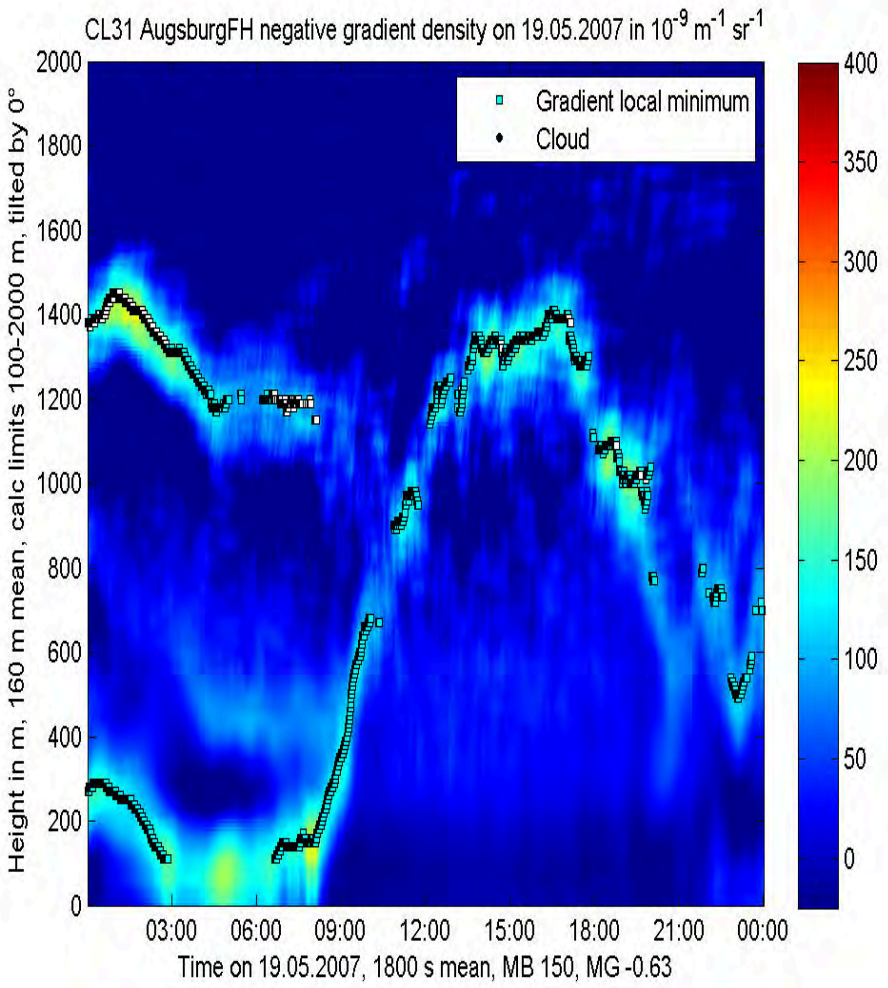

Algorithm to detect MLH from Ceilometer-Daten

criterion

minimal vertical gradient of backscatter intensity (the most negative gradient)

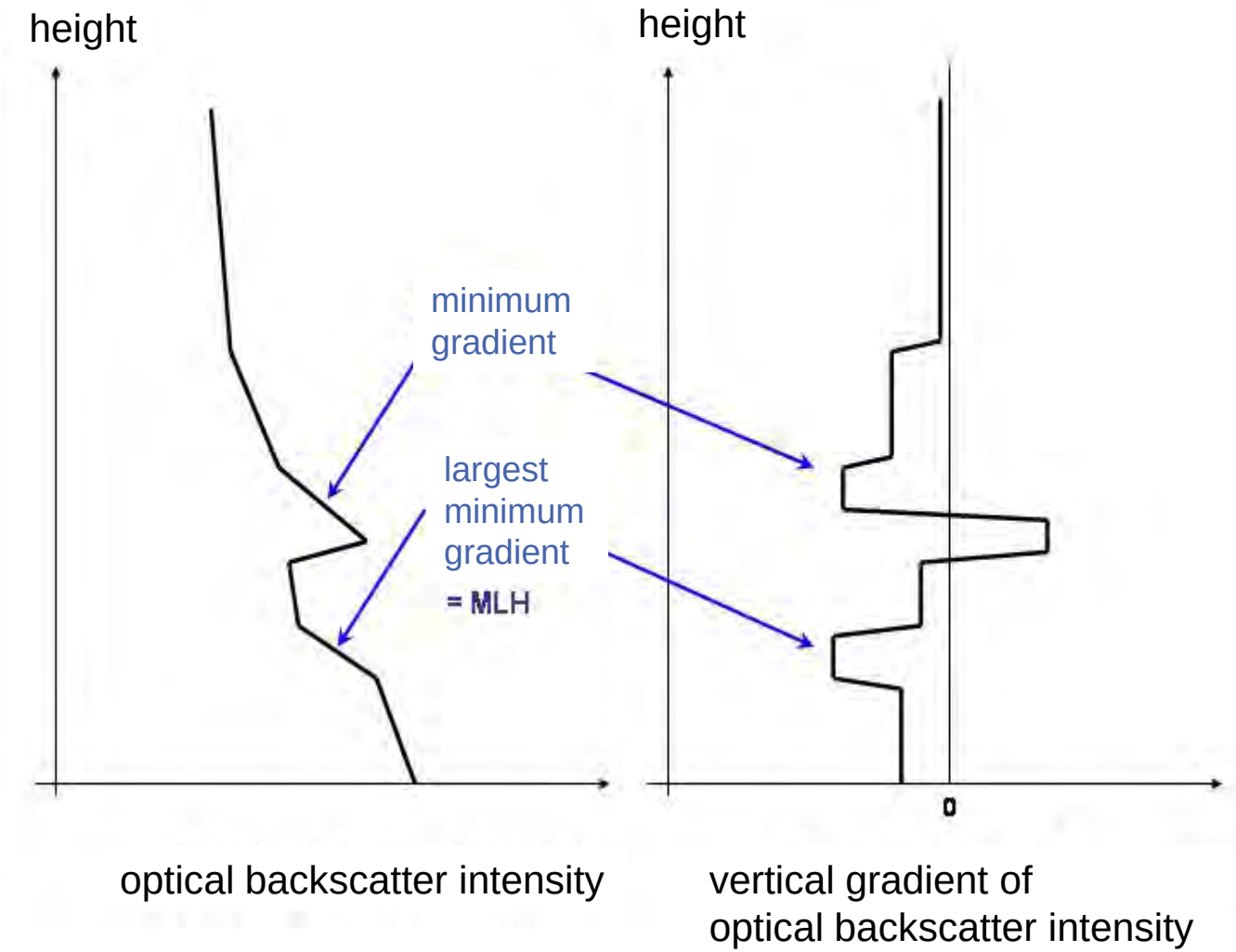

Different gradient methods (see Sicard et al. 2006, BLM 119, 135-157)

logarithmic gradient minimum

gradient minimum

inflection point method
(minimum of 2nd derivative)

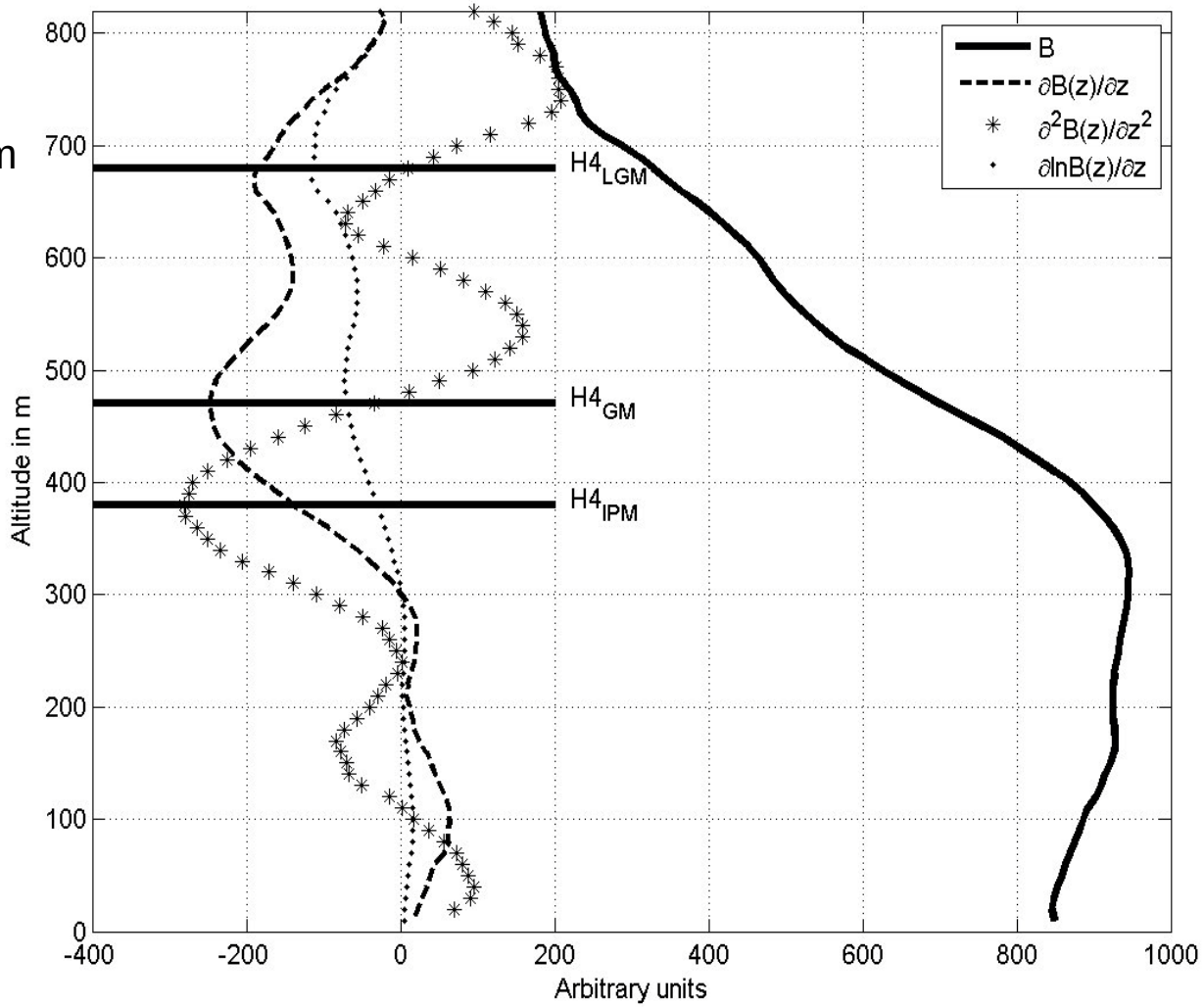

comparison of two different ceilometers

LD40

two optical axes
- wave length: 855 nm
- height resolution: 7.5 m
- max. range: 13000 m

CL31 / CL51

one optical axis
- wave length: 905 nm
- height resolution: 5 m
- max. range: 7500 m

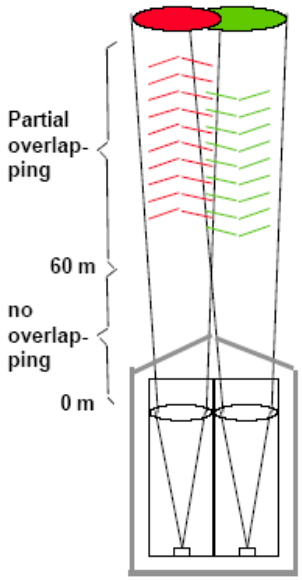

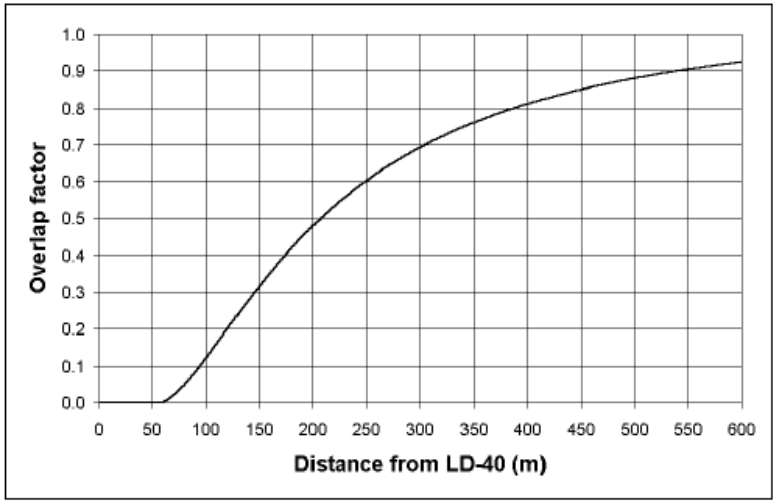

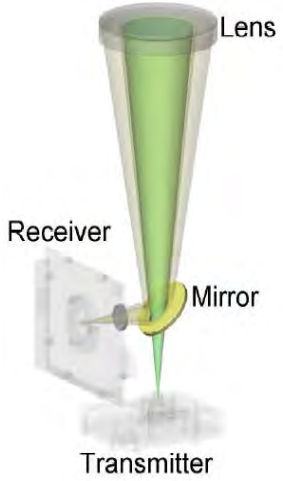

comparison of LD40 and CL31

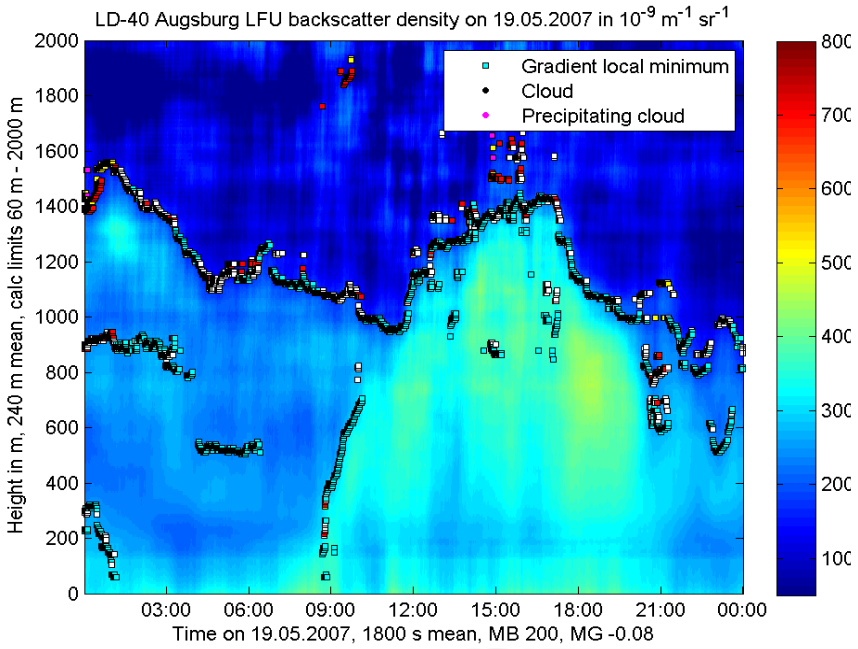

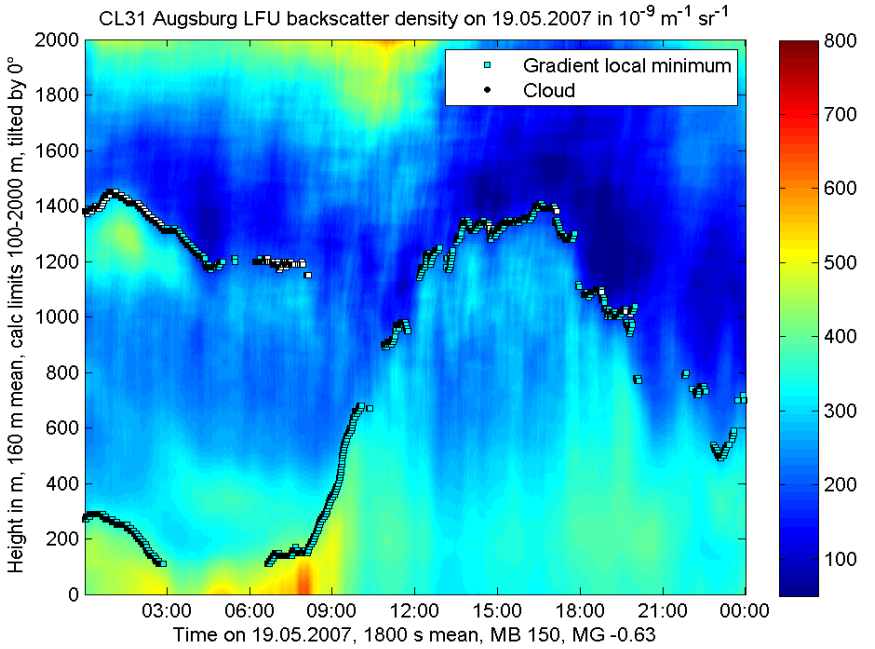

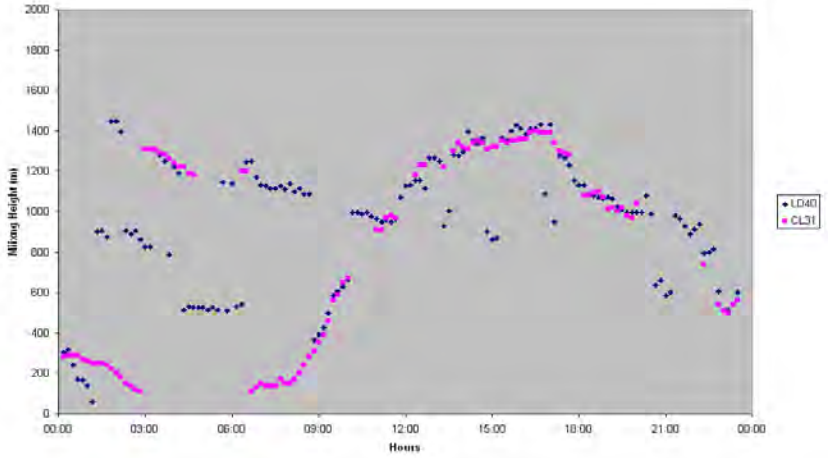

Eyjafjallajökull ash cloud over Southern Germany

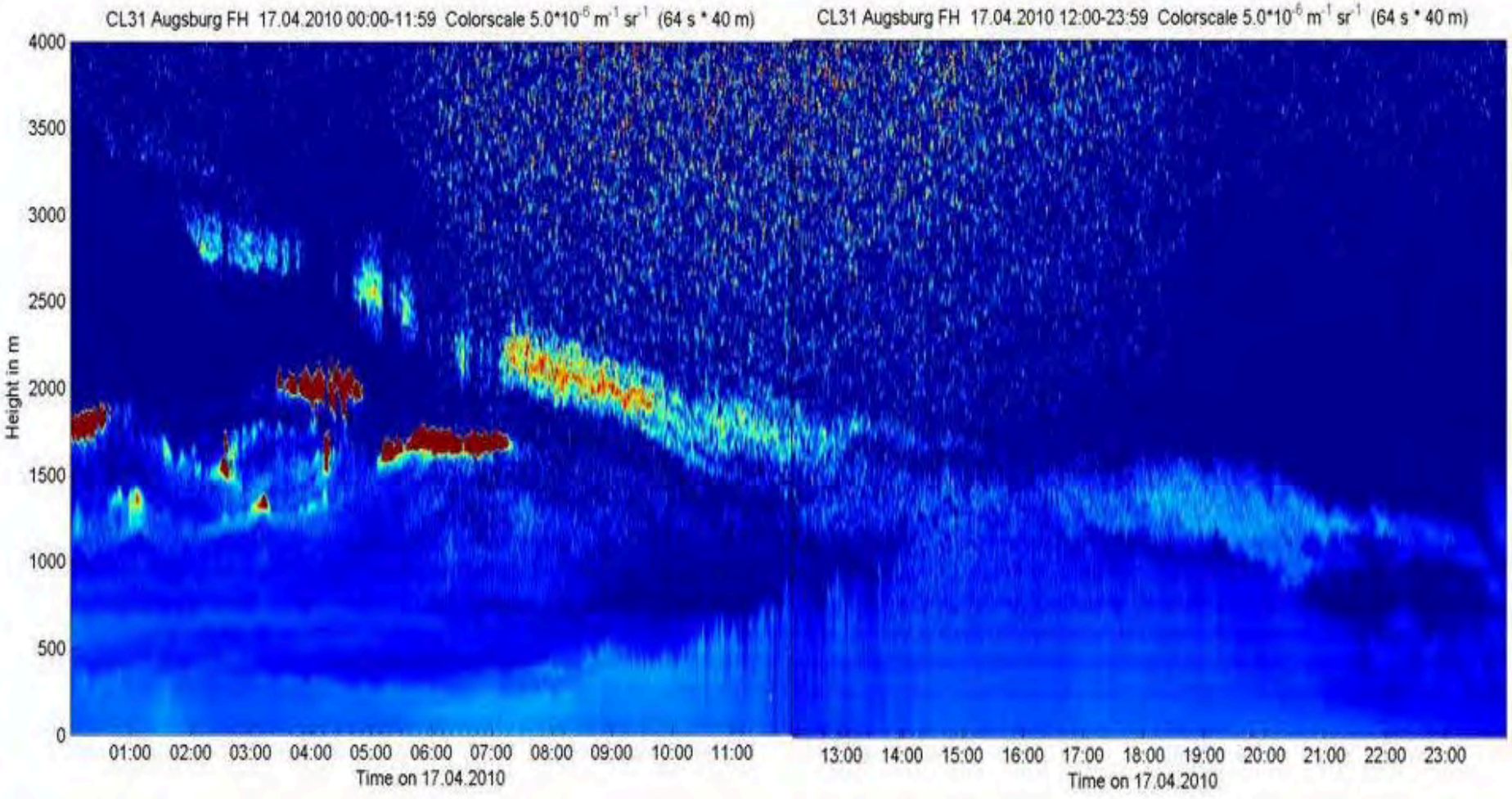

read more: Emeis, S., R. Forkel, W. Junkermann, K. Schäfer, H. Flentje, S. Gilge, W. Fricke, M. Wiegner, V. Freudenthaler, S. Groß, L. Ries, F. Meinhardt, W. Birmili, C. Münkel, F. Obleitner, P. Suppan, 2011: Measurement and simulation of the 16/17 April 2010 Eyjafjallajökull volcanic ash layer dispersion in the northern Alpine region. Atmos. Chem. Phys., 11, 2689–2701

RASS

principles of operation

examples

stefan.emeis@kit.edu Institute for Meteorology and Climate Research – Atmospheric Environmental Research

RASS measuring principle

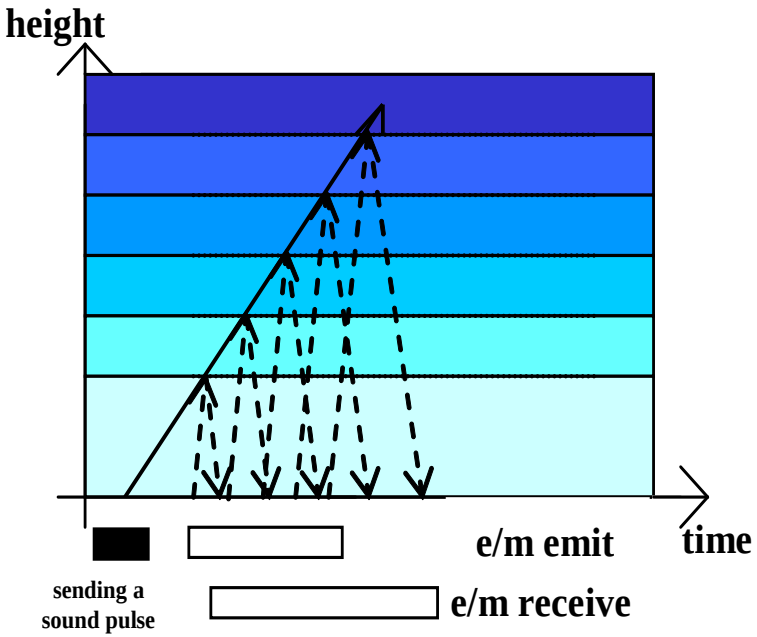

detection:

travel time of em./ac. signal	= height	
ac. backscatter intensity	= turbulence	(identical to SODAR)
ac. Doppler-shift	= line-of-sight wind speed	(identical to SODAR)
em. Doppler shift	= sound speed ➔ temperature	

RASS (radio-acoustic remote sensing)

measures vertical temperature profiles

Bragg-RASS: windprofiler plus acoustic component

Doppler-RASS: SODAR plus electro-magnetic component

UHF RASS (boundary layer)

VHF RASS (troposphere)

RASS: frequencies

Bragg condition:
acoustic wavelength = ½ electro-magnetic wavelength

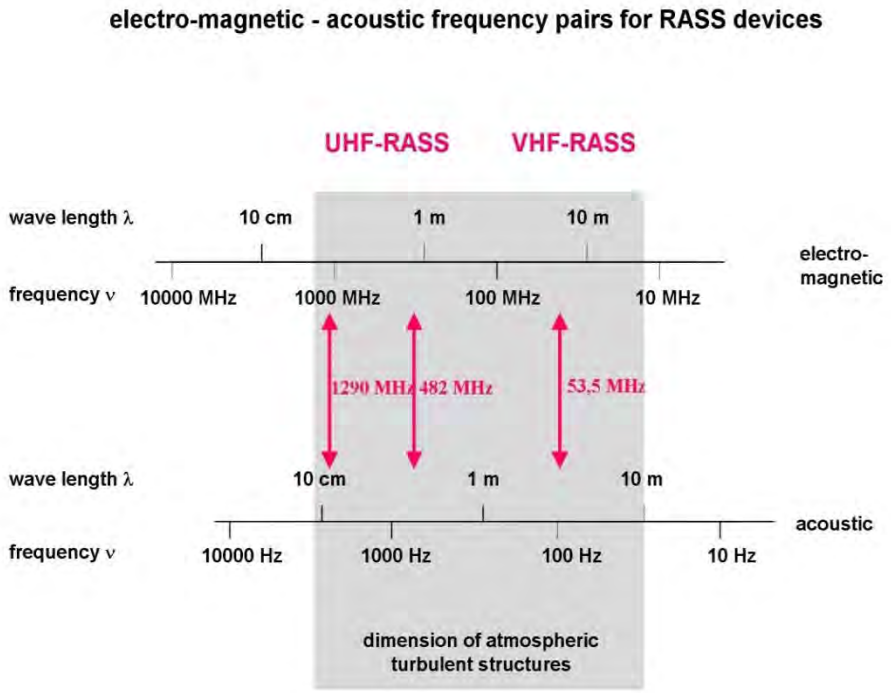

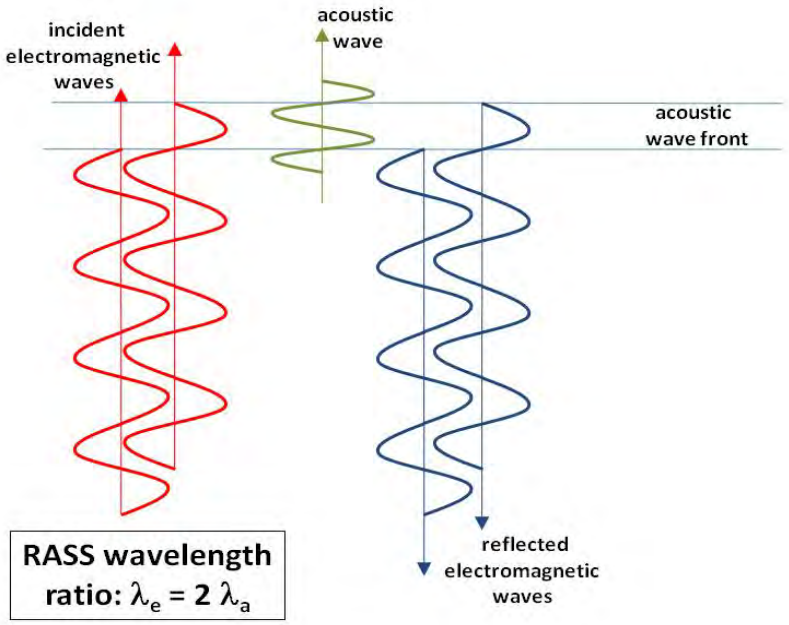

Emeis, S., 2010: Measurement Methods in Atmospheric Sciences - In situ and remote. Borntraeger, Stuttgart, 272 pp., 103 figs, 28 tables, ISBN 978-3-443-01066-9.

SODAR-RASS
(Doppler-RASS)

(METEK)

acoustic frequ.: 1077 Hz
radio frequ.: 474 MHz
resolution: 20 m
lowest
range gate: ca. 40 m

vertical range: 540 m

Bragg-RASS

acoustic frequ.: about 3000 Hz
radio frequ.: 1290 MHz
resolution: 50 m
lowest
range gate: ca. 200 m

vertical range: 1000 m

example RASS data: summer day
potential temperature (left), horizontal wind (right)

300 m

40 m

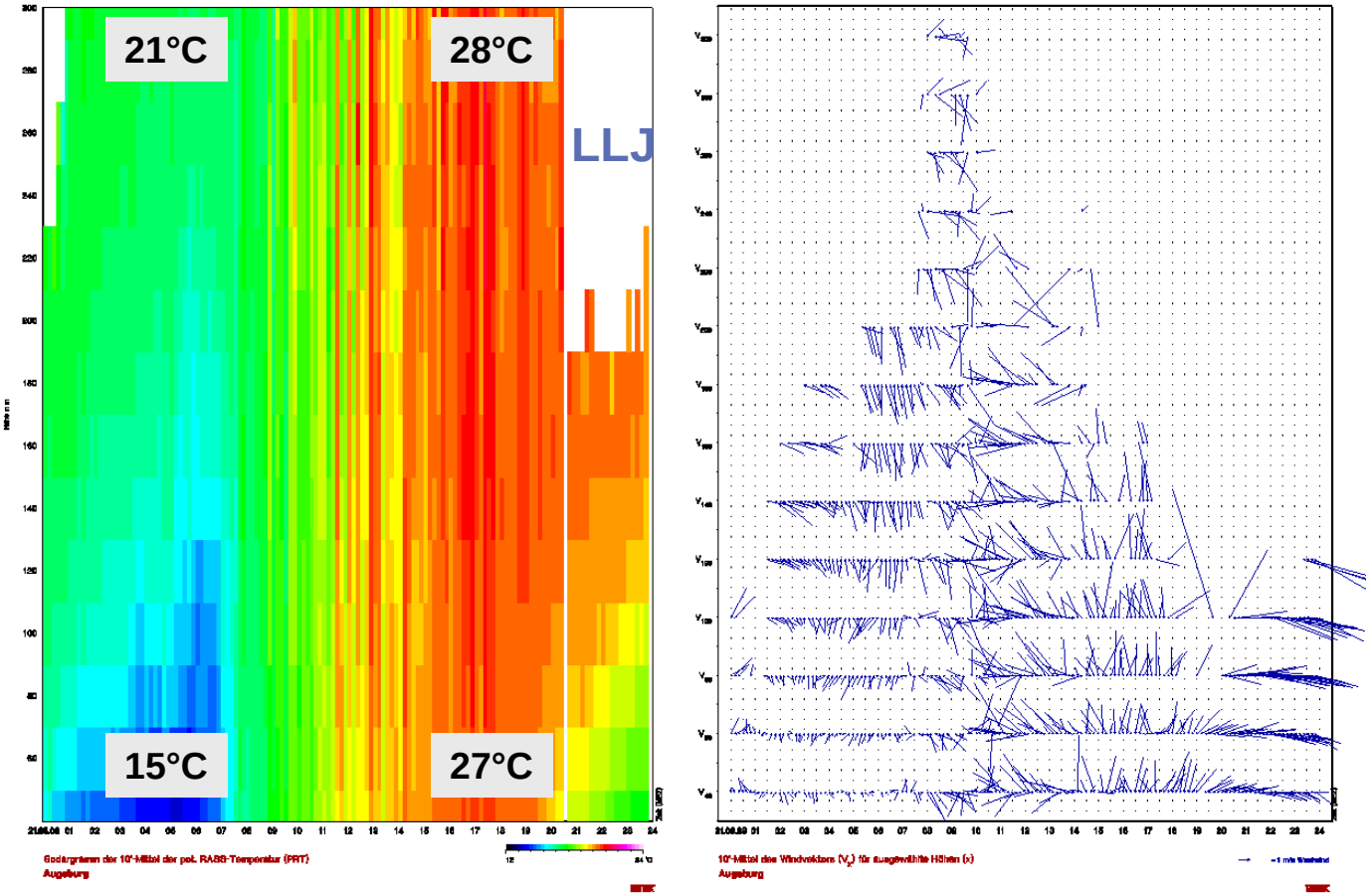

example RASS data: winter day
potential temperature (left), horizontal wind (right)

300 m

40 m

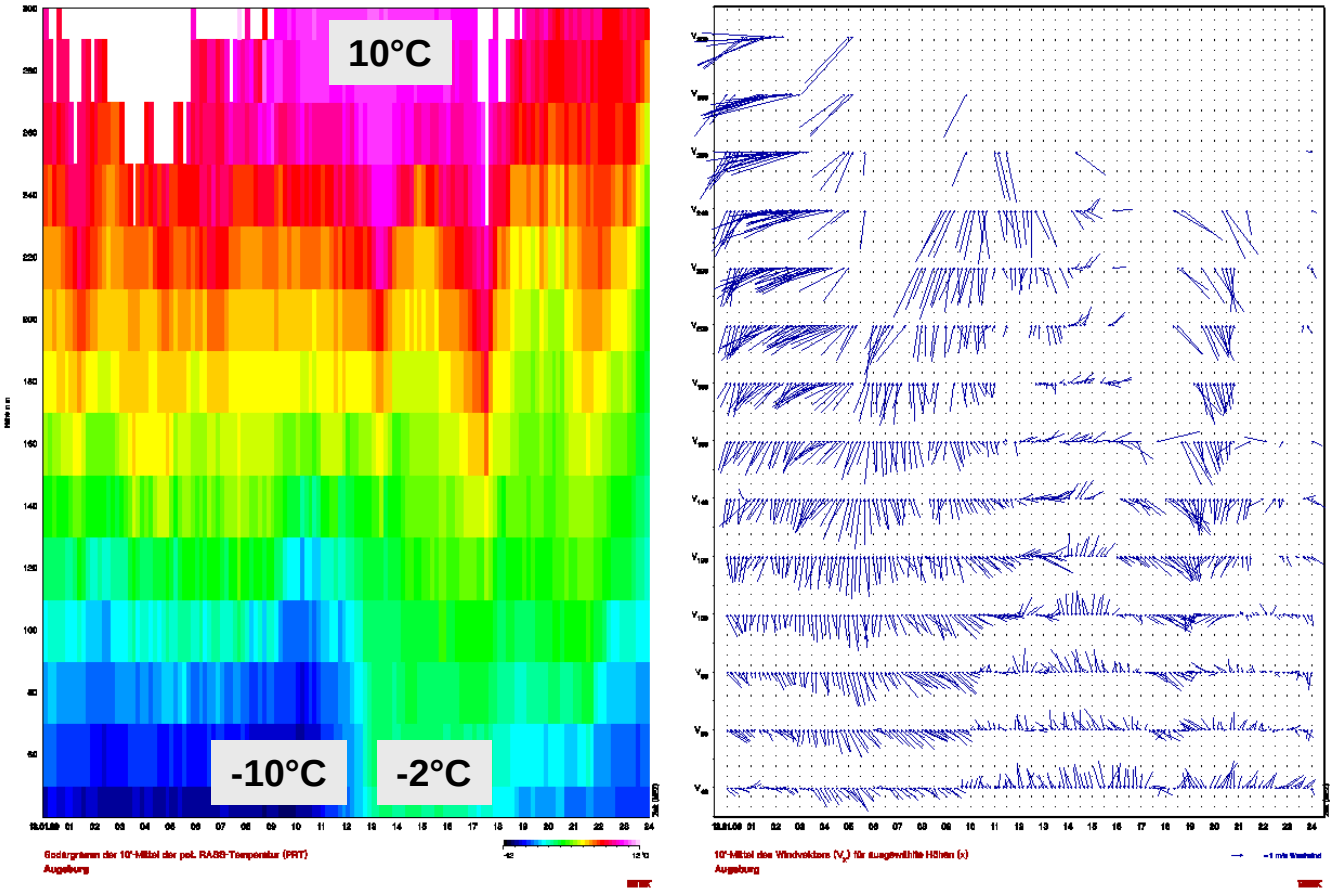

example RASS data: inversion
potential temperature (left), horizontal wind (right)

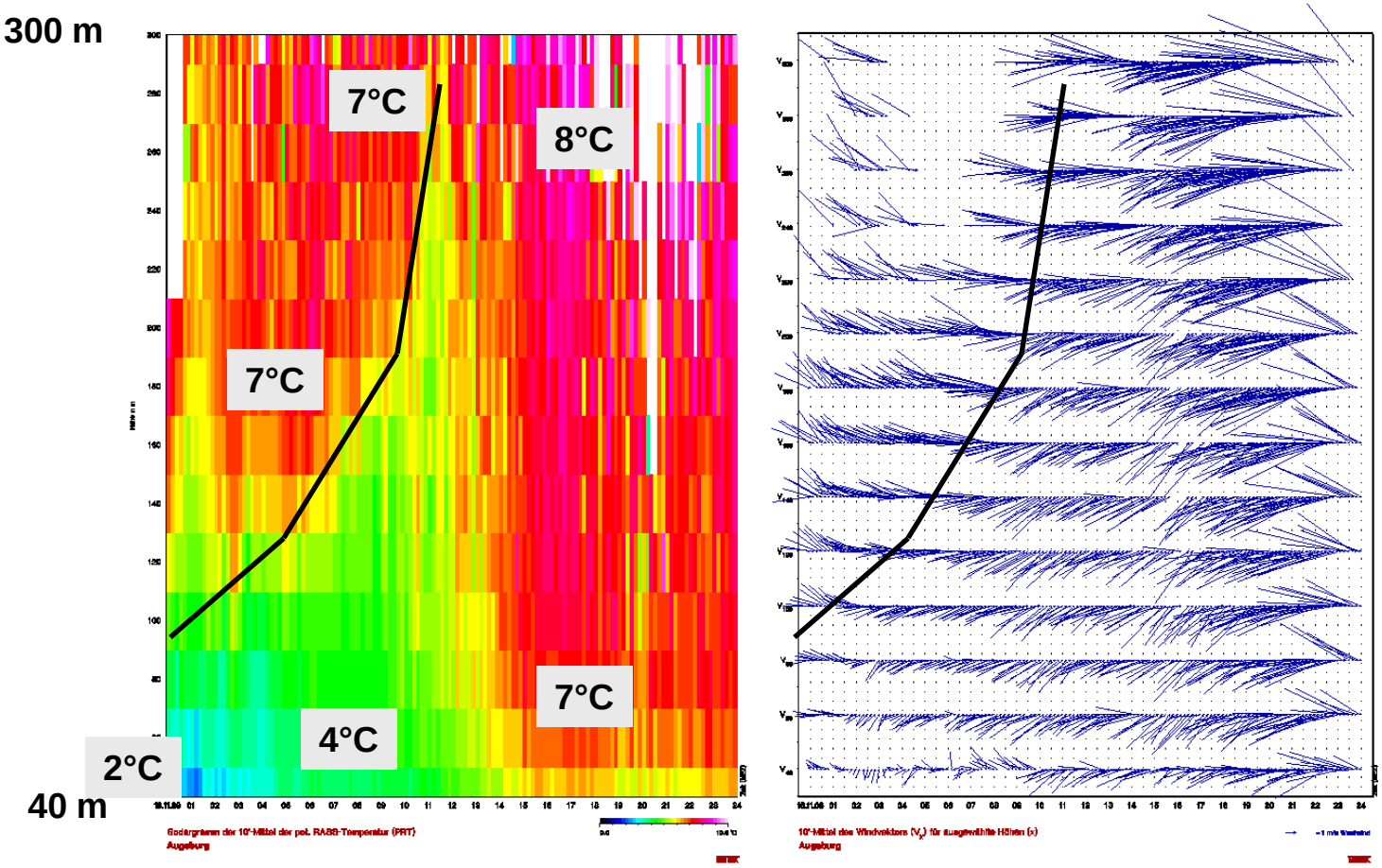

Doppler windlidar

wind, turbulence, aerosol detection, mixing-layer height, low-level jet

stefan.emeis@kit.edu Institute for Meteorology and Climate Research – Atmospheric Environmental Research

Doppler windlidar measuring principle

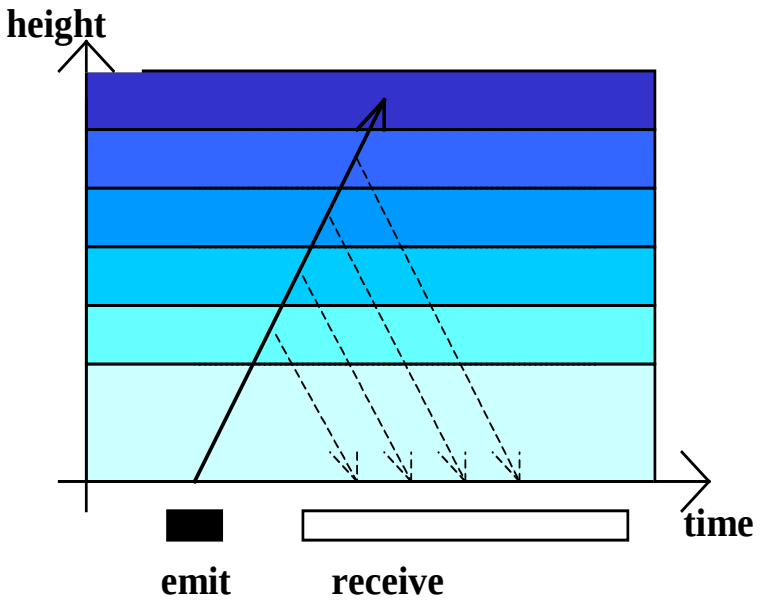

detection:

travel time of signal = height
backscatter intensity = particle size and number distribution
depolarisation = particle shape
Doppler-shift = wind speed in the line of sight

mobile Doppler windlidar from Halo Photonics

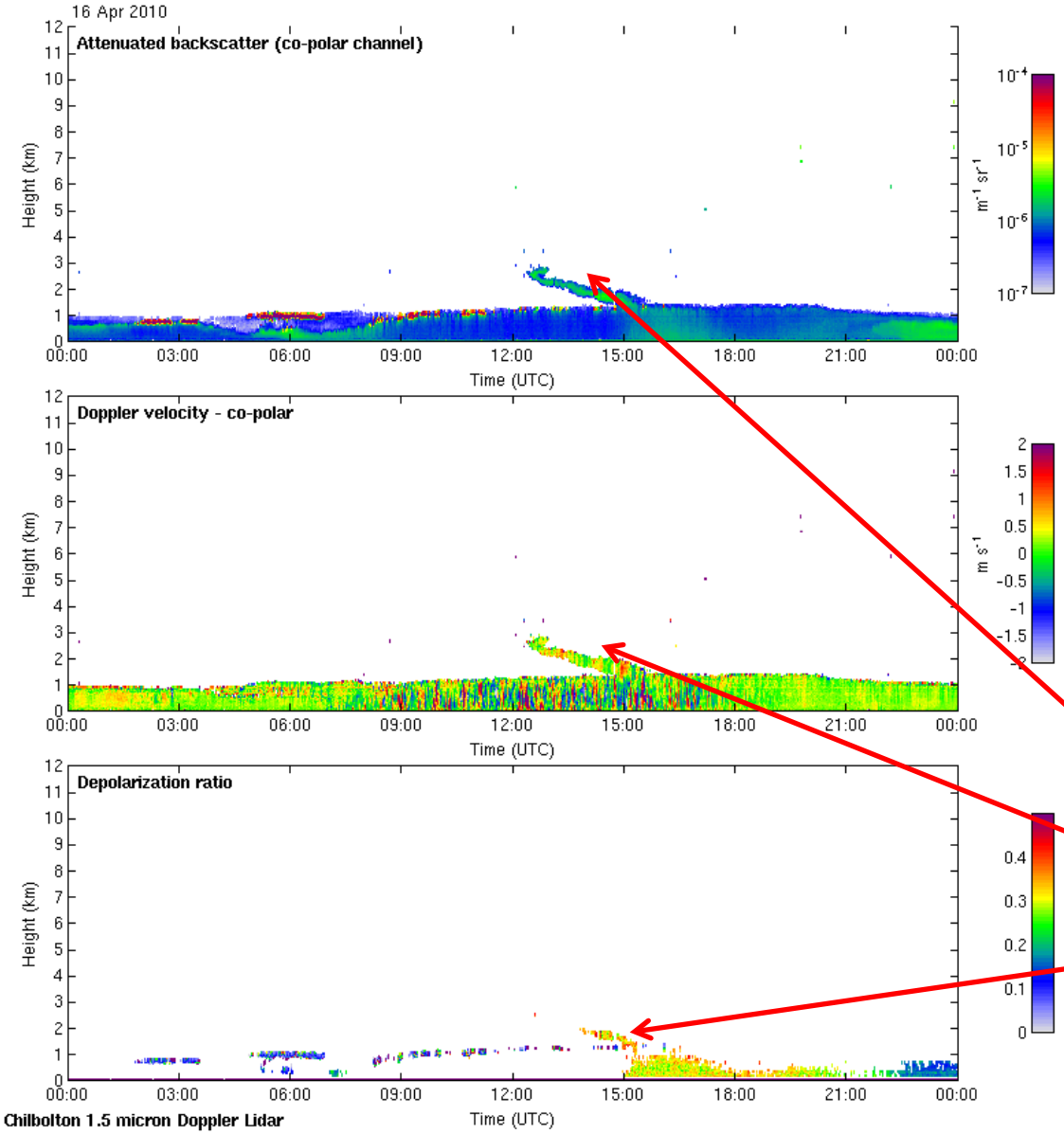

sample data from windlidar

April 16, 2010

by Univ. of Reading

taken at

Chilbolton, UK

http://www.met.reading.ac.uk/radar/realtime/archive/doppler-lidar/20100416_chilbolton_halo-doppler-lidar.png

volcanic ash from Eyjafjallajokull

realtime data: http://www.chilbolton.rl.ac.uk/weather/lidar.htm

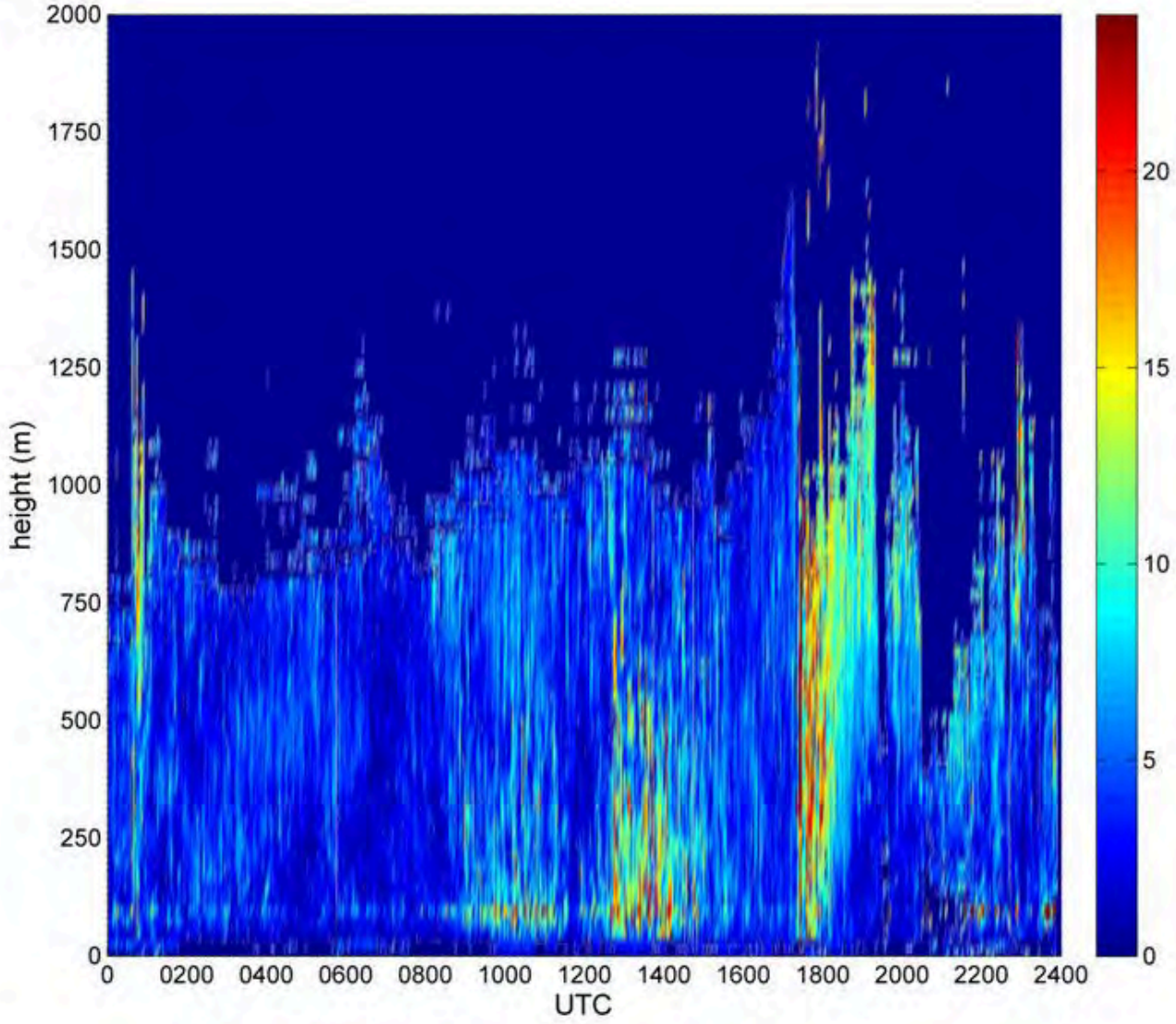

sample data from windlidar

wind speeds in m/s (colour bar)

June 22, 2011

by IMK-IFU

taken at

Garmisch-Partenk., Germany

Comparisons between different instruments

temperature profile and aerosol backscatter

comparison of RASS data (potential temperature, right) with aerosol backscatter from a ceilometer (left)

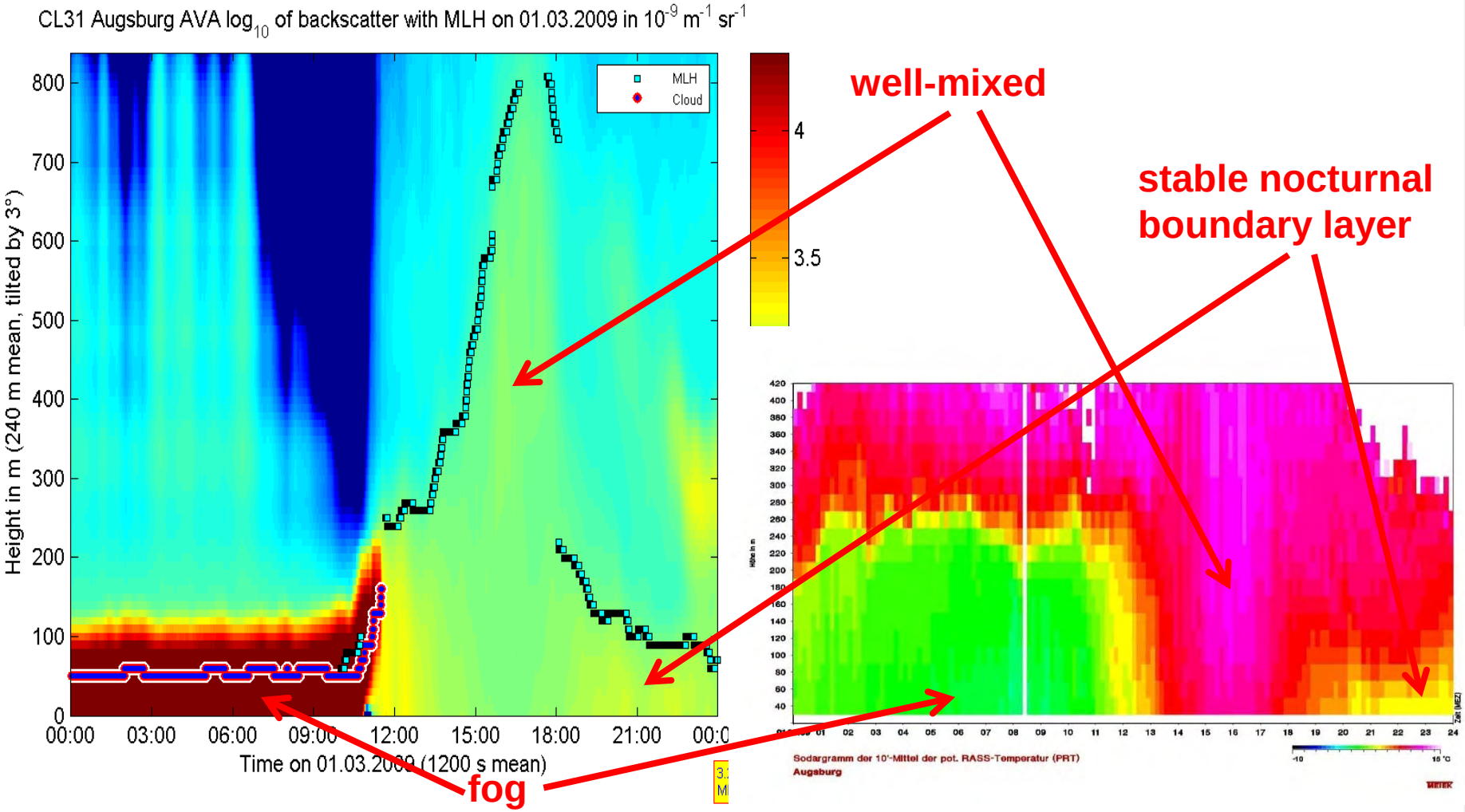

Detection of the diurnal variation of PBL structure from SODAR and Ceilometer data taken in Budapest

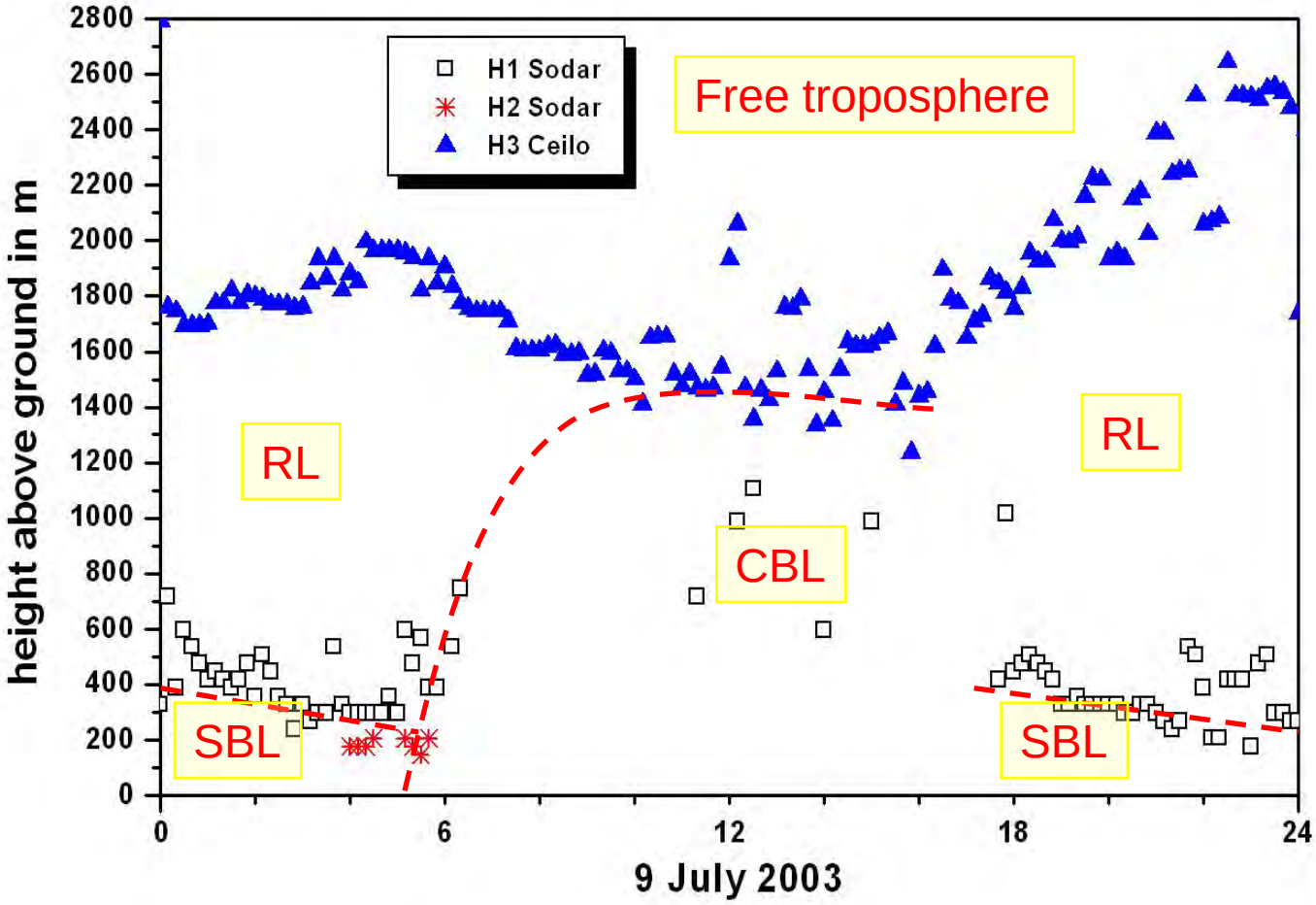

SBL:

stable boundary layer (usually at night and in winter)

CBL:

convective boundary layer (usually at daytime due to strong insolation)

RL:

residual layer (usually at nighttime)

Emeis, S., K. Schäfer, 2006: Remote sensing methods to investigate boundary-layer structures relevant to air pollution in cities. Bound.-Lay Meteorol., 121, 377-385,

Differences in MLH detection from SODAR and Ceilometer data taken in Budapest

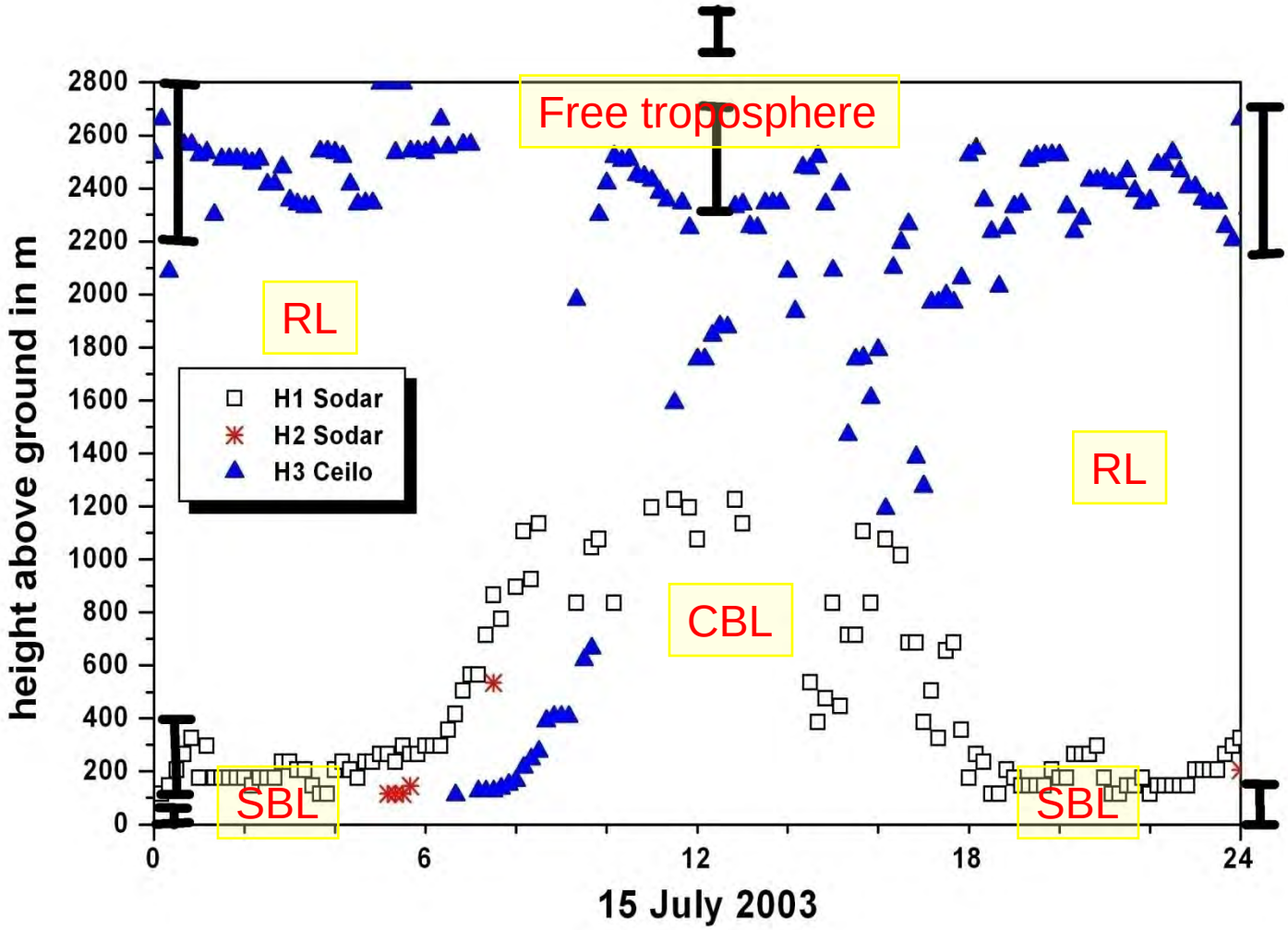

inversions derived from radiosonde data

Emeis, S., K. Schäfer, 2006: Remote sensing methods to investigate boundary-layer structures relevant to air pollution in cities. Bound.-Lay Meteorol., 121, 377-385,

RASS data Augsburg February 2009

potential temperature (top), backscatter SODAR (middle), Ceilometer (bottom)

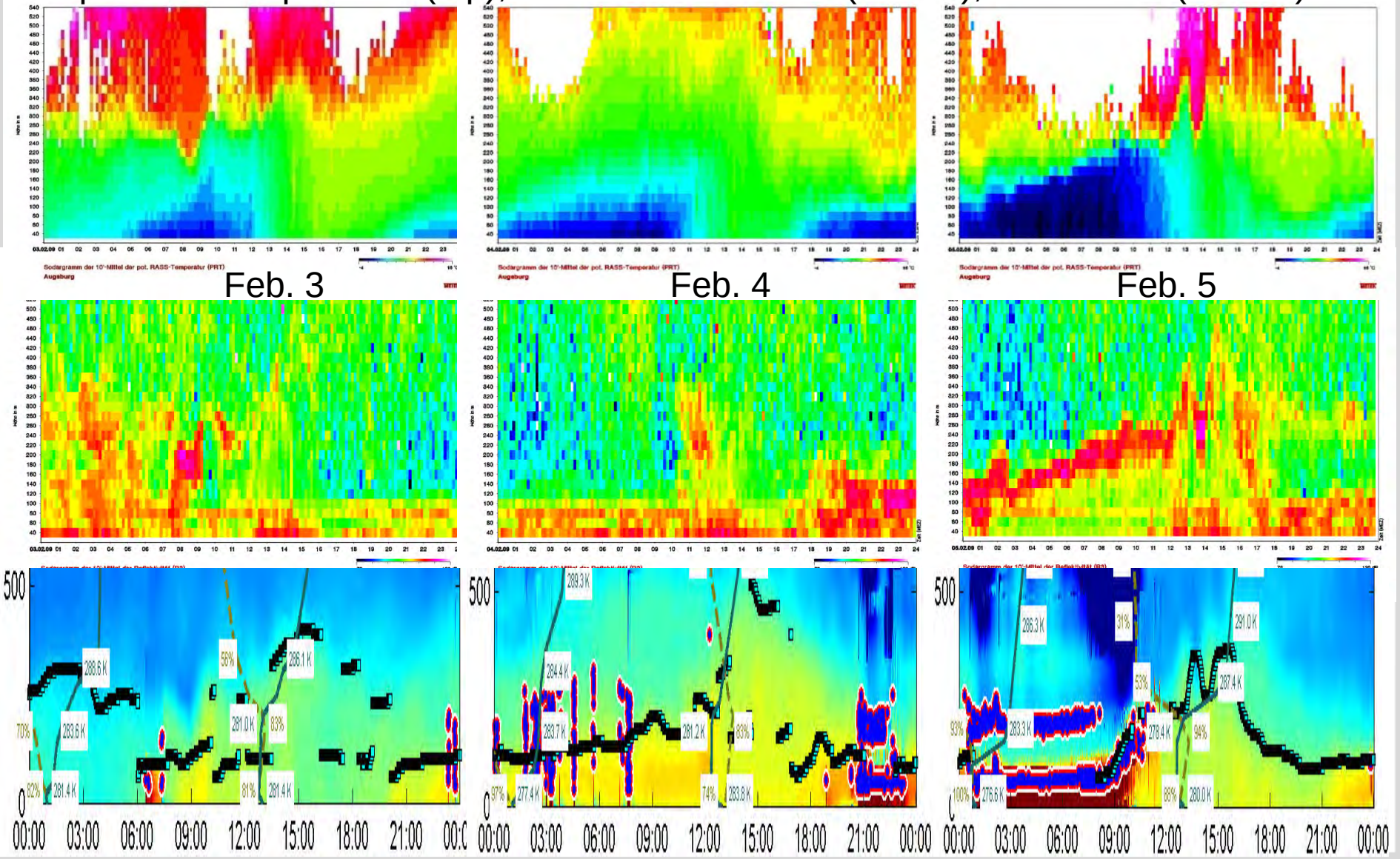

RASS data Augsburg February 2009

potential temperature (top), MLH RASS (middle), MHL SODAR/Ceilo (bottom)

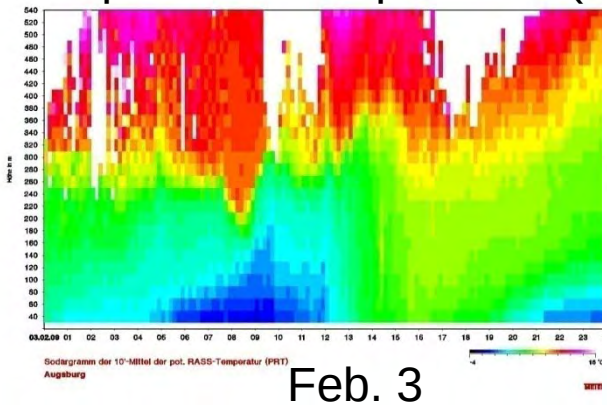

Feb. 3

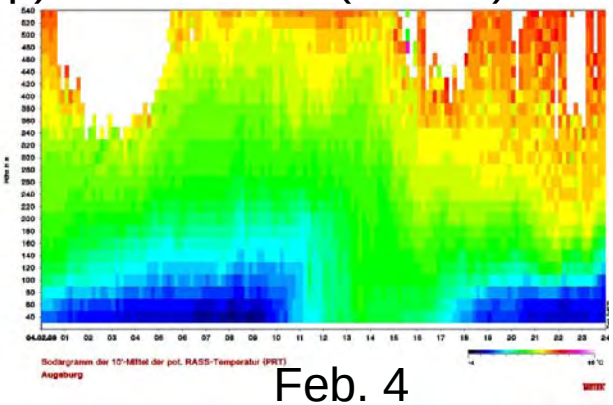

Feb. 4

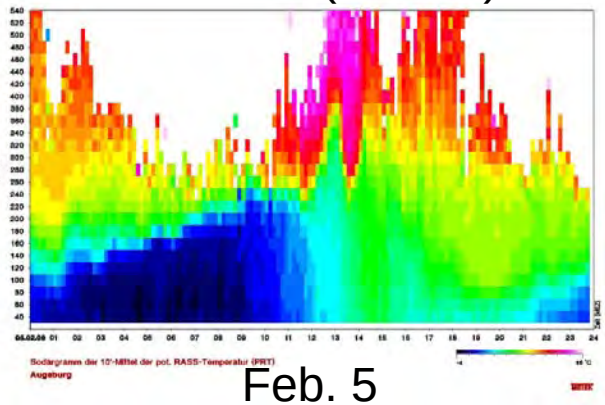

Feb. 5

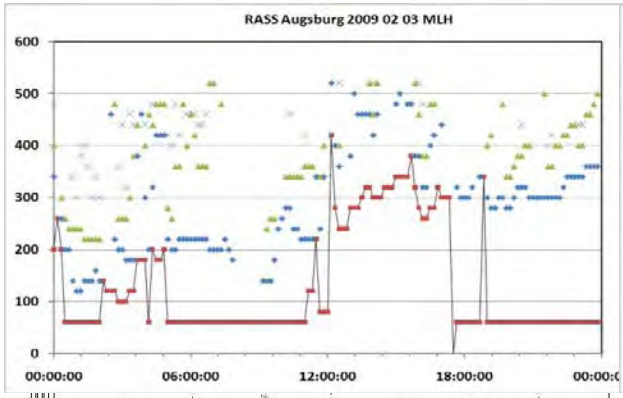

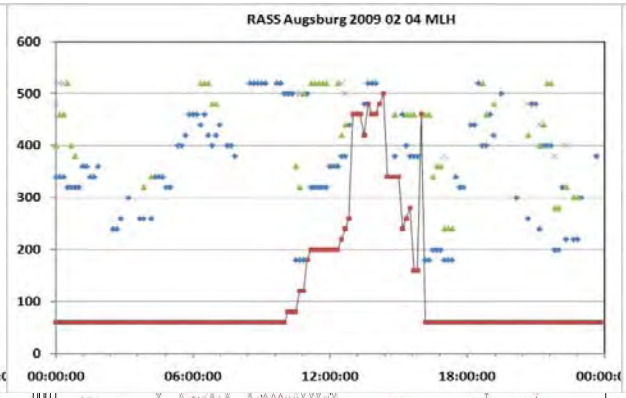

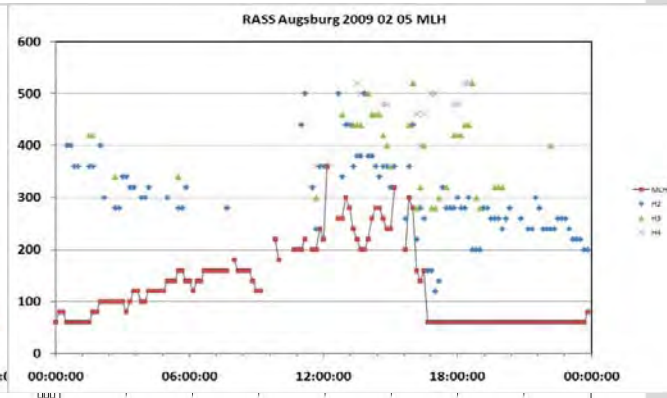

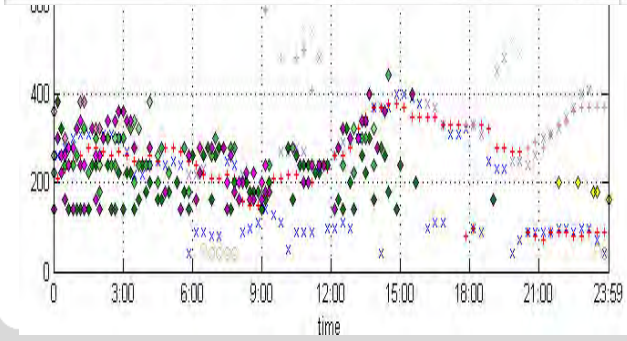

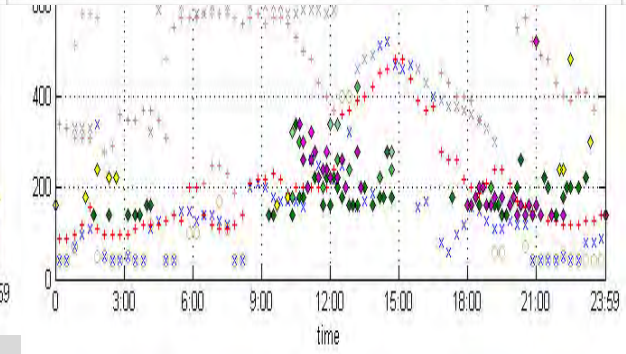

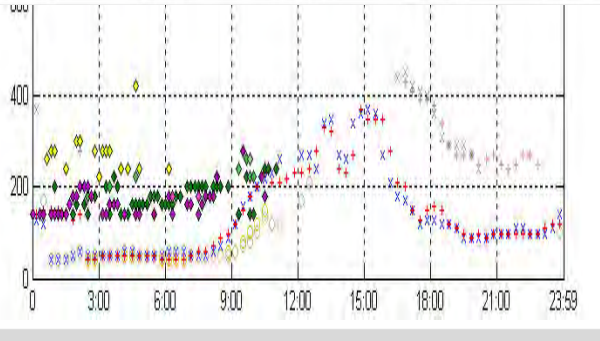

Summary

 stefan.emeis@kit.edu Institute for Meteorology and Climate Research – Atmospheric Environmental Research

Clicker question:

Which instrument is best?

A **sodar**

B **ceilometer**

C **wind lidar**

D **RASS**

E **don’t know**

quality criteria:

data availability

vertical range

direct/indirect detection

Doppler analysis

☺ ☺ ☺ 💣 **RASS delivers temperature profiles, wind profiles are additionally available.**
MLH directly from temperature profiles. LLJ from wind profiles.
Does not work properly under high wind speeds. Restricted range.

☺ ☺ ☺ 💣 **wind lidar detects wind profiles, aerosol distribution and water droplets. It has to be assumed that the aerosol follows the thermal structure of the atmosphere and the wind.**
MLH from aerosol backscatter, wind speed variance, LLJ from wind profiles.
Does not work properly in extreme clear (aerosol-free) air and during precipitation events and fog.

☺ ☺ 💣 💣 **Ceilometer detects aerosol distribution and water droplets. It has to be assumed that the aerosol follows the thermal structure of the atmosphere.**
MLH indirectly from aerosol backscatter using a MLH algorithm.
Does not work properly in extreme clear (aerosol-free) air and during precipitation events and fog.

☺ 💣 💣 💣 **SODAR detects wind profiles, temperature fluctuations and gradients, but no absolute temperature.**
MLH indirectly from acoustic backscatter (MLH algorithm). LLJ from wind profiles.
Does not work properly under perfectly neutral stratification, with very high wind speeds, and during stronger precipitation events. Restricted range.

Literature

SODAR:

Asimakopoulos, D.N., C.G. Helmis, J. Michopoulos, 2004: Evaluation of SODAR methods for the determination of the atmospheric boundary layer mixing height. - Meteor. Atmos. Phys. 85, 85–92.

Beyrich, F., 1997: Mixing height estimation from sodar data – a critical discussion. - Atmos. Environ. 31, 3941–3953.

Ceilometer:

Schäfer, K., S.M. Emeis, A. Rauch, C. Münkel, S. Vogt, 2004: Determination of mixing-layer heights from ceilometer data. In: Remote Sensing of Clouds and the Atmosphere IX. Schäfer, K., A. Comeron, M. Carleer, R.H. Picard, N. Sifakis (Eds.), Proc. SPIE, Bellingham, WA, USA, Vol. 5571, 248–259.

Sicard, M., C. Pérez, F. Rocadenbosch, J.M. Baldasano, D. García-Vizcaino, 2006: Mixed-Layer Depth Determination in the Barcelona Coastal Area From Regular Lidar Measurements: Methods, Results and Limitations. - Bound.-Lay. Meteor. 119, 135–157.

RASS:

Engelbart, D.A.M., J. Bange, 2002: Determination of boundary-layer parameters using wind profiler/RASS and sodar/RASS in the frame of the LITFASS project. Theor. Appl. Climatol. 73, 53–65.

Emeis, S., K. Schäfer, C. Münkel, 2009: Observation of the structure of the urban boundary layer with different ceilometers and validation by RASS data. Meteorol. Z., 18, 149-154. (Open access, freely available from http://dx.doi.org/10.1127/0941-2948/2009/0365)

Emeis, S., K. Schäfer, C. Münkel, R. Friedl, P. Suppan, 2011: Evaluation of the interpretation of ceilometer data with RASS and radiosonde data. Bound.-Lay. Meteorol., online April 5, 2011. DOI: 10.1007/s10546-011-9604-6

Windlidar:

Emeis, S., M. Harris, R.M. Banta, 2007: Boundary-layer anemometry by optical remote sensing for wind energy applications. - Meteorol. Z., 16, 337-347.

Reviews:

Emeis, S., K. Schäfer, C. Münkel, 2008: Surface-based remote sensing of the mixing-layer height – a review. - Meteorol. Z., 17, 621-630. (Open access, freely available from http://dx.doi.org/10.1127/0941-2948/2008/0312)

Books:

Wind energy meteorology

Emeis, S., 2012: Wind Energy Meteorology - Atmospheric physics for wind power generation. Springer Heidelberg etc., to appear in autumn 2012.

boundary-layer remote sensing with application examples:

Emeis, S., 2011: Surface-Based Remote Sensing of the Atmospheric Boundary Layer. Series: Atmospheric and Oceanographic Sciences Library, Vol. 40. Springer Heidelberg etc., X+174 pp. 114 illus., 57 in color., H/C. ISBN: 978-90-481-9339-4, DOI: 10.1007/978-90-481-9340-0

overview on the entire range of meteorological measurement methods:

Emeis, S., 2010: Measurement Methods in Atmospheric Sciences. In situ and remote. Series: Quantifying the Environment Vol. 1. Borntraeger Stuttgart. XIV+257 pp., 103 Figs, 28 Tab. ISBN 978-3-443-01066-9.

Karlsruhe Institute of Technology

WINDFORS
Wind Energy
Research Alliance

Horns Rev wake clouds explained

Stefan Emeis
stefan.emeis@kit.edu

INSTITUTE OF METEOROLOGY AND CLIMATE RESEARCH, Atmospheric Environmental Research

Photo: Vattenfall/C. Steiness

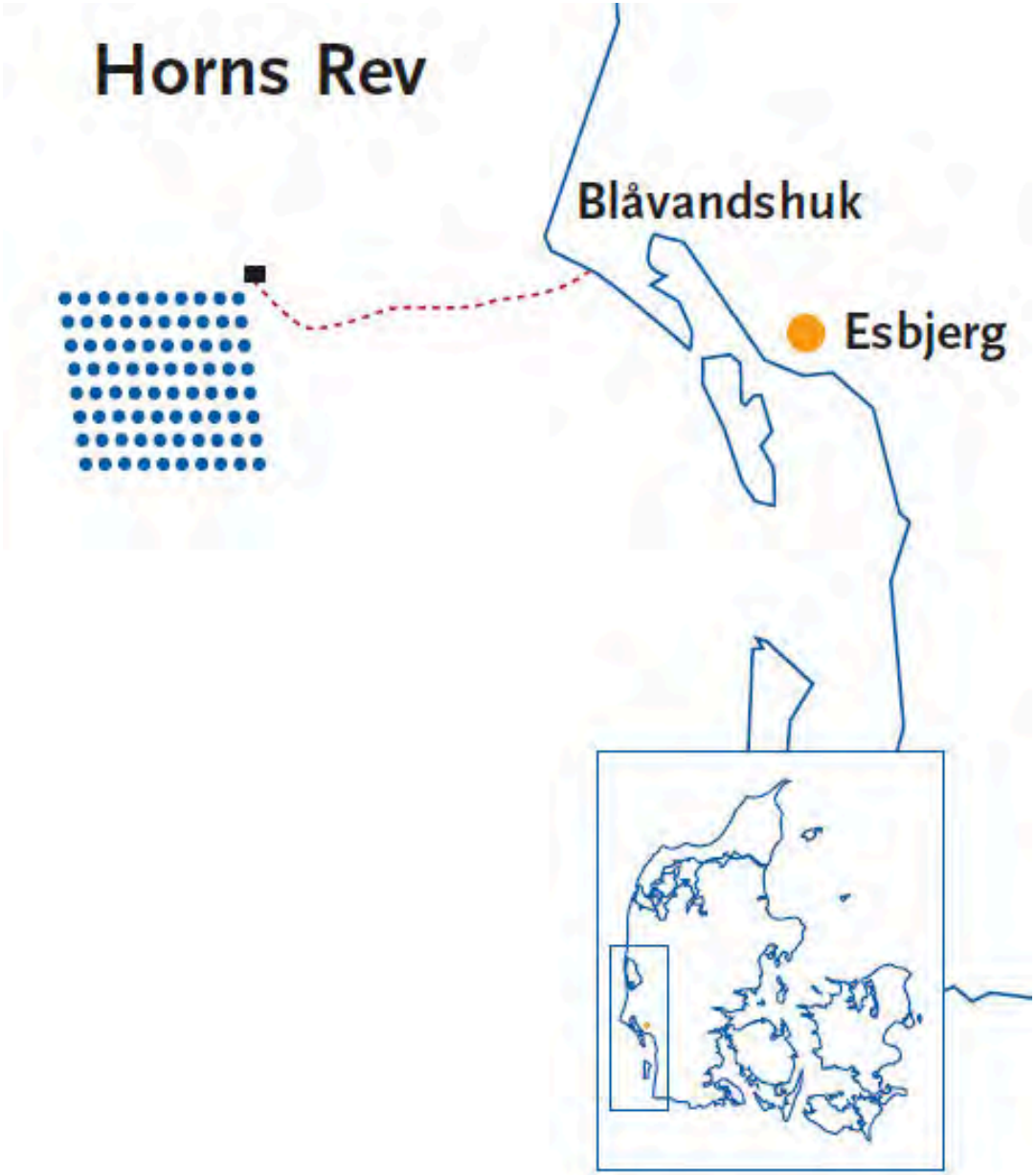
Horns Rev
Blåvandshuk
Esbjerg

10 m wind

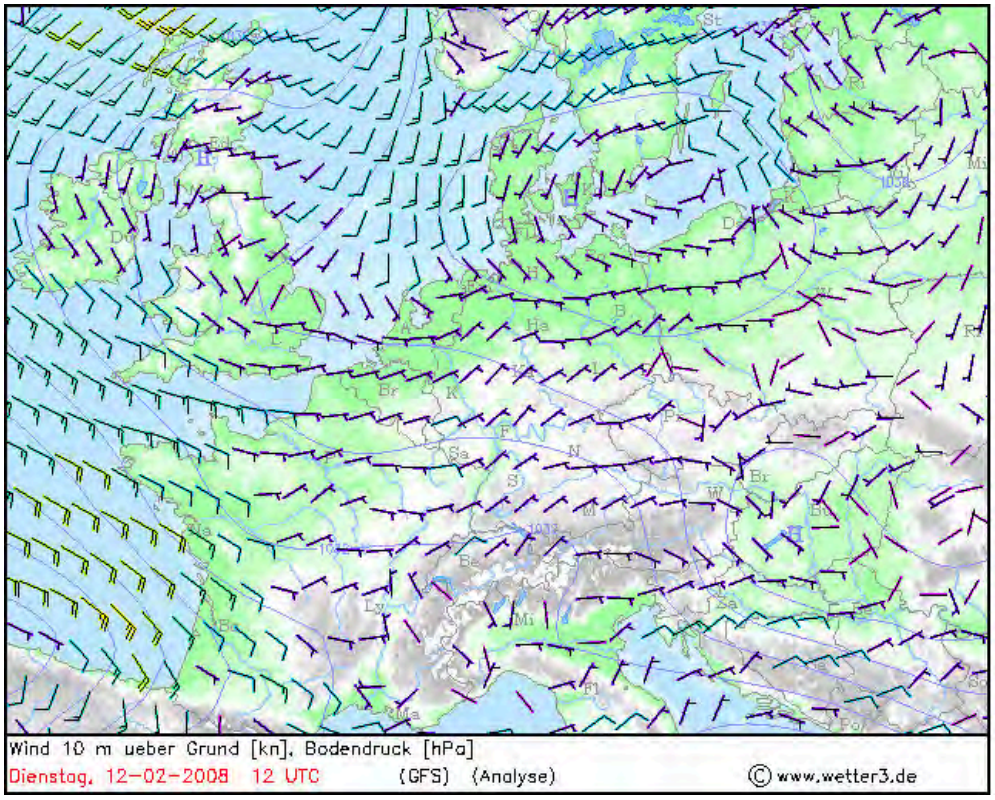

SST (°C)

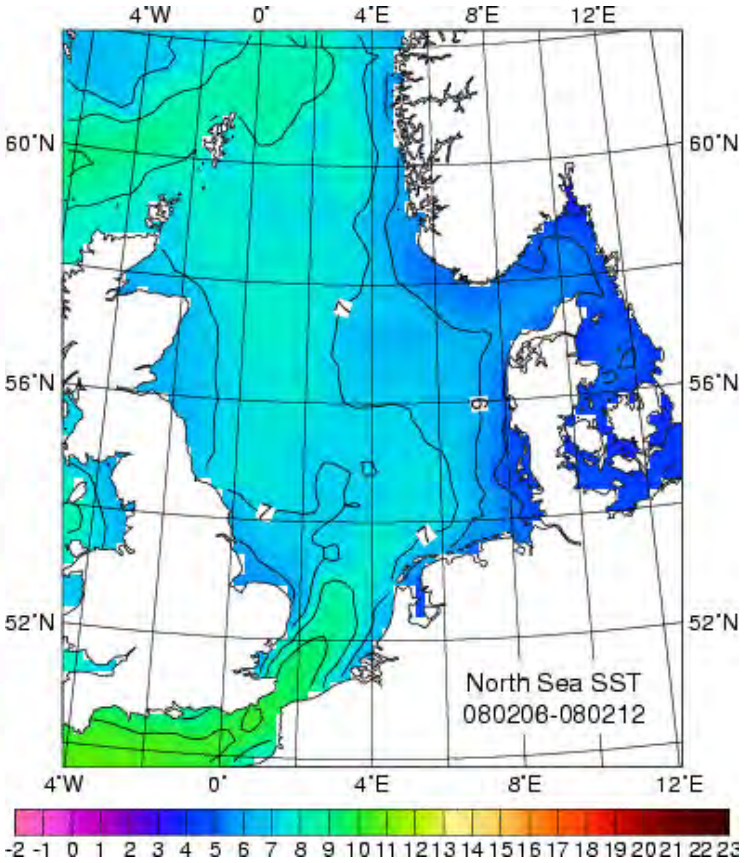

explanation of wake clouds: mixing fog on February 12, 2008

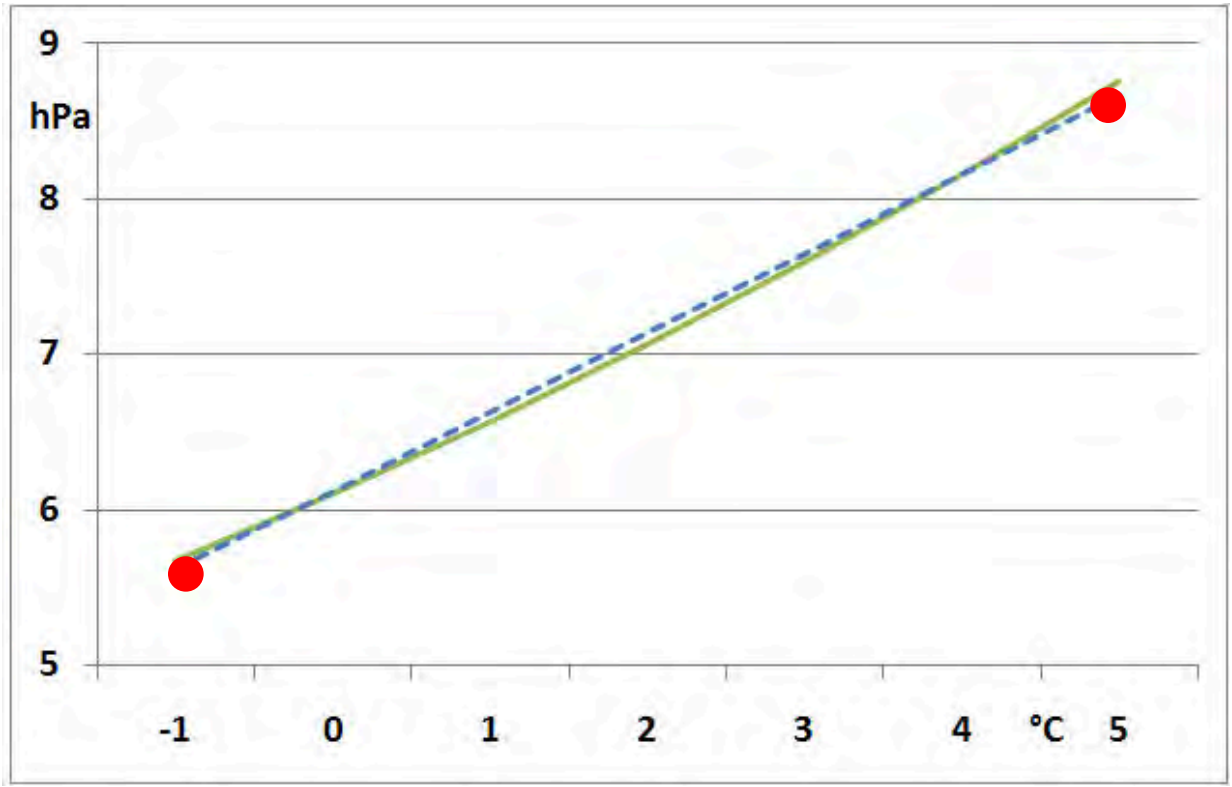

air directly over the water: 5°C, more than 99% relative humidity
air at hub height: -1°C, more than 99% relative humidity
after mixing: 2°C, above 101% humidity ➔ clouds

explanation of wake clouds: mixing fog on February 12, 2008

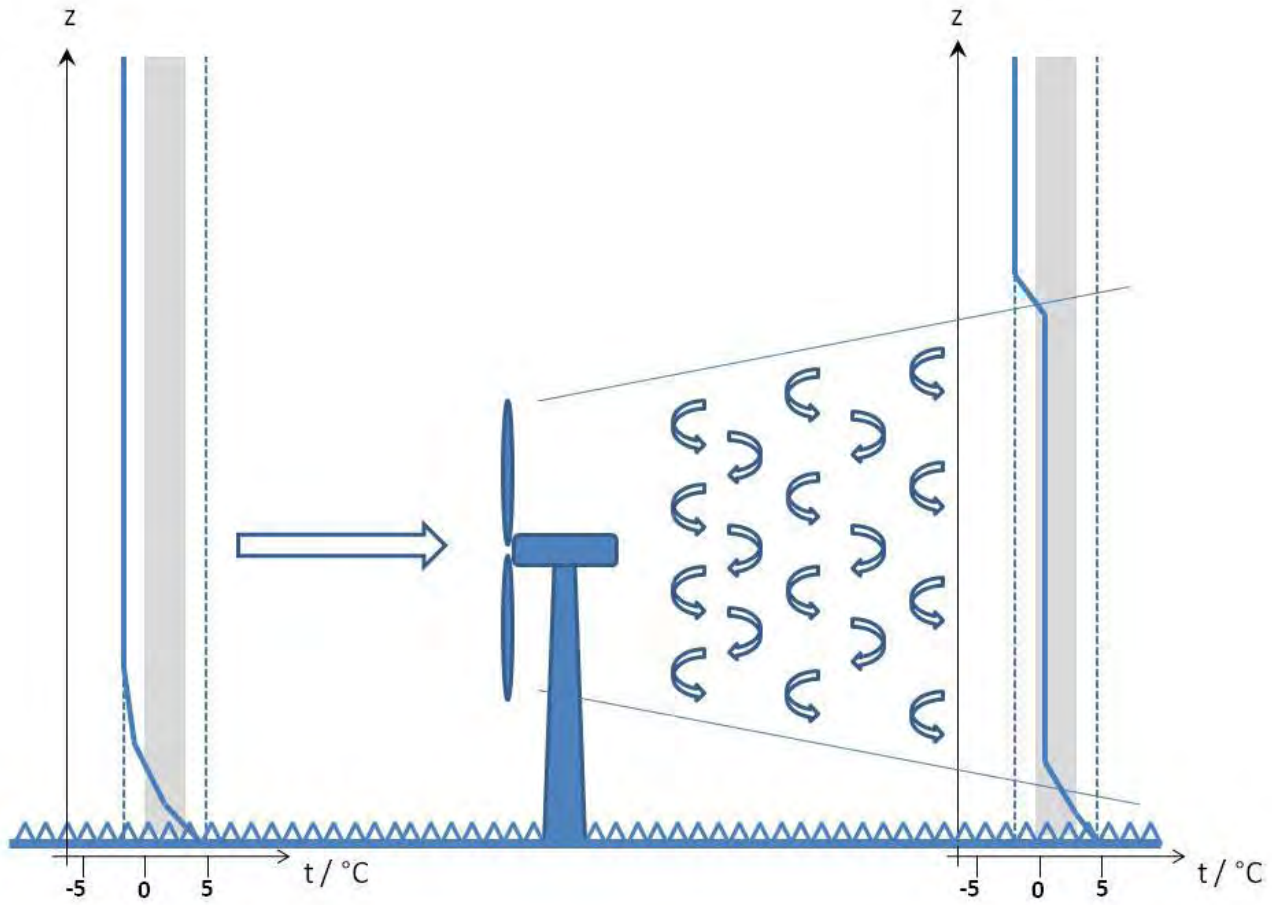

air directly over the water: 5°C, more than 99% relative humidity
air at hub height: -1°C, more than 99% relative humidity
after mixing: 2°C, above 101% humidity ➔ clouds

Photo: Vattenfall/C. Steiness


Photo: Vattenfall/C. Steiness

DEWI Magazine 37 (August 2010), 52-55

http://www.dewi.de/dewi/fileadmin/pdf/publications/Magazin_37/07.pdf

Thank you very much for your attention